DESIGN AND TESTING OF AN H2/O2 PREDETONATOR FOR A SIMULATED

ROTATING DETONATION ENGINE CHANNEL

THESIS

Stephen J. Miller, 2Lt, USAF

AFIT-ENY-13-M-23

DEPARTMENT OF THE AIR FORCE
AIR UNIVERSITY

AIR FORCE INSTITUTE OF TECHNOLOGY

Wright-Patterson Air Force Base, Ohio

AFIT-ENY-13-M-23

DESIGN AND TESTING OF AN H2/O2 PREDETONATOR FOR A SIMULATED

ROTATING DETONATION ENGINE CHANNEL

THESIS

Presented to the Faculty

Department of Aeronautical and Astronautical Engineering

Graduate School of Engineering and Management

Air Force Institute of Technology

Air University

Air Education and Training Command

in Partial Fulfillment of the Requirements for the

Degree of Master of Science in Aeronautical Engineering

Stephen J. Miller, B.S.A.E.

2Lt, USAF

March 2013

AFIT-ENY-13-M-23

DESIGN AND TESTING OF AN H2/O2 PREDETONATOR FOR A SIMULATED ROTATING DETONATION ENGINE CHANNEL

Stephen J. Miller, B.S.A.E.
2Lt, USAF

Approved:

_____   _____
Paul I. King (Chairman)   Date

_____   _____
Frederick R. Schauer (Member)   Date

_____   _____
Marc D. Polanka (Member)   Date

AFIT-ENY-13-M-23

Abstract

A study is presented on the relationship between a pre-detonator and a detonation channel of an RDE. Testing was conducted on a straight narrow channel made of clear polycarbonate windows connected to an H2/O2 pre-detonator to simulate the RDE initiation scheme and allow for flow visualization. A comparison is made on decoupling distance and wave velocities for a range of pre-detonator designs, inclination angles, equivalence ratios and geometries placed within the simulated channel. Regardless of inclination angle or equivalence ratio the detonation wave decoupled within 25 mm from the pre-detonator exit into the channel. A step change in diameter 25 mm from the exit of the pre-detonator increased the coupled distance to approximately 40 mm from the pre-detonator exit. A step diameter change also increased the exit velocity of the wave and directionalized the flow. Wedges of 30°, 45° and 60°, placed in the channel next to the pre-detonator exit, increased the distance the shock and flame remained coupled from the pre-detonator exit to 42 mm, 50 mm and 60 mm, respectively.

Acknowledgments

I am incredibly grateful for the opportunity to attend the Air Force Institute of Technology and to be able to conduct research in the Detonation Engine Research Facility. This opportunity has provided me with a strong admiration for the amount of time and effort required to conducted research and development for the Air Force. I would like to thank Dr. Paul King for his help in the preparation of testing and guidance in writing in my paper. Additionaly much thanks to Dr. Marc Polanka for sitting on my committee as well as providing several helpful edits to improve my paper and its overall readability.

I would also like to thank Dr. Fred Schauer and Dr. John Hoke for sharing their knowledge on PDEs, and allowing me to play in their lab. I also owe a great deal of thanks to Chris Stevens. He was willing to help out fabricating parts, setting up tests and checking over results. Chris was also willing to answer all of my questions and without his help this research would not have been possible. Additionally I would like to thank Curt Rice and Justin Goffena for helping to set up tests and fabricate parts. I would also like to thank the rest of the crew in D-bay for helping to critique my work and provide guidance whenever it was needed.

Finally I thank my amazing fiance, Ali, for her willingness to read over my paper, as well as put up with discussions on the inner workings of MatLab.

Stephen J. Miller

Table of Contents

List of Figures

List of Tables

List of Symbols

Symbol	Definition
a	Speed of sound
B	Bias uncertainty
d_c	Critical diameter (mm)
D_{CJ}	Chapman-Jouguet velocity (m/s)
M	Mach number
p	Precision uncertainty
P	Pressure (Pa)
h	Specific enthalpy (J/g)
q	Difference between enthalpy of formation of reactants and products
$R_{specific}$	Specific gas constant (J / (kg*K))
T	Temperature (K)
u	Velocity (m/s)
γ	Ratio of specific heats
δ_x	Change in x-direction (m)
δ_t	Time step (s)
θ_{crit}	Critical angle for transition from Mach to regular reflection
θ_w	Angle of wedge
ρ	Density (g/m^3)
λ	Cell size (mm)
σ	Standard deviation
ϕ	Equivalence ratio
ω	Angle of incidence shock to the flow

List of Acronyms

Acronym	Definition
CJ	Chapman-Jouguet
DDT	Deflagration-to-Detonation Transition
DERF	Detonation Engine Research Facility
fps	frames per second
ID	Inner Diameter
OD	Outer Diameter
PDE	Pulse Detonation Engines
RDE	Rotating Detonation Engine
WPAFB	Wright Patterson Air Force Base
ZND	Zeldovich, von Neumann and Doring

DESIGN AND TESTING OF AN H2/O2 PREDETONATOR FOR A SIMULATED

ROTATING DETONATION ENGINE CHANNEL

I. Introduction

As the United States government enacts stricter budgetary limitations, the Air Force

must continue to adapt to meet the same mission requirements with less resources

available. Innovative solutions are needed to cut fuel use, while still meeting the demands

of high performance aircraft. One of those solutions involves the use of a Pulse

Detonation Engines (PDE) to reduce fuel consumption and maintenance costs.

Traditional gas turbine engines utilize a process known as deflagration to burn fuel.

Deflagration is subsonic, and is modeled as a constant pressure process. When used in

engines, combustors that use deflagration require compressors to raise the pressure before

burning and subsequently entering the turbine. PDEs are a pressure rise process that use a

detonation wave to complete the burning of fuel. The pressure rise combustion provides a

weight reduction and maintenance savings from the reduced compressor stages. The

ability to integrate detonations waves into a gas-turbine engine require the creation of a

reliable Rotating Detonation Engine (RDE) design. An RDE is a circular narrow chamber

in which a detonation wave propagates circumferentially for as long as fuel and air are

provided. Several problems still exist though, and must be solved before RDEs can be

integrated to modern engines.

1.0.1 Motivation

This thesis focuses on the startup problem presented by the RDE. The RDE

detonation wave starts through the use of a pre-detonator which is oriented tangentially to

the main chamber. Although one would expect the detonation wave to continue in the

pre-detonator direction, often the wave will proceed in the opposite direction, split in two directions or not transition to detonation at all. RDE implementation in future applications require a reliable and consistent starting process. Currently, there is far too much variability to implement the RDE in a real application

1.0.2   Research Objectives

The goal of this thesis is to examine and understand the relationship between the pre-detonator and the RDE. The first part of the research focuses on what is currently happening in the time between ignition of the pre-detonator and when a detonation wave successfully circles the RDE channel. The second part of the research focuses on ways to achieve reliable and replicable startup of the RDE. The purpose of this research was to develop a means to consistently start the RDE and get a detonation wave to travel in the same direction every start.

There were four tests conducted to complete the research. The first of the tests was conducted on a straight narrow channel connected to a pre-detonator designed to replicate the RDE channel (Sec. 4.1). Further examination of the pre-detonator was necessary after seeing the detonation wave decouple upon entering the narrow channel. The pre-detonators were tested with a carved spiral cut at the entrance to facilitate the creation of detonation waves (Sec. 4.2). The goal of the second test was to create a detonation front as early as possible in the pre-detonator tube. A nozzle shape at the entrance was shown to produce the most consistent detonation location. The third round of testing then placed the nozzle shape at the pre-detonator exit to see its effect on exit velocity of the shock wave. The goal of the third test was to achieve the highest shock wave exit velocities from the pre-detonator (Sec. 4.3). The fourth round of testing examined the redesigned pre-detonator on the original narrow channel. In addition to testing the pre-detonator, wedges were placed into the channel (Sec. 4.4). The goal of the final round of testing was to produce a coupled detonation front in one direction while simultaneously

decoupling the detonation front in the opposing direction.

The final round of testing produced consistent detonation waves and achieved travel in one direction upon entering the simulated channel. This work has been presented at both the 51st AIAA Aerospace Sciences Meeting and at the 38th Dayton-Cincinnati Aerospace Sciences Symposium.

II.   Literature Review

This chapter will cover both the mechanics of detonation waves and previous research that has been conducted. A history of detonation waves is provided as a means to orient the reader to what a detonation is. The history also shows the extent to which detonation research has accelerated in recent years (Sec. 2.1). The mechanics of a detonation wave are provided to facilitate the readers understanding of the differences between a deflagration, shock wave and detonation wave, as well as the theories behind detonations (Sec. 2.3). After covering the basics behind detonations, a discussion on the operation of RDEs is provided. The RDE section will cover the basic theories of the engines, as well as the limitations and issues that must be solved before implementation in real applications (Sec. 2.4). A discussion is also provided as to how different researchers have attempted to solve the starting problem presented by RDEs (Sec. 2.5). In addition to RDE research, a background is provided on the behavior of detonation waves around corners (Sec. 2.6). The diffraction section provides insight as to how the detonation wave behaves exiting the pre-detonator tube and traveling into the channel. Finally a more recent study is provided to show the ability of wedges to re-ignite decoupled detonation fronts traveling through a channel (Sec. 2.7). The wedges are relevant to the current research, as they were eventually used in this research with the desire to achieve the same results of re-ignition.

2.1   History

Devices such as the PDE and the RDE have primarily been studied over the last 50 years, however research dates as far back as the late 19th century with the first measurement of detonation velocities of guncotton charges by Abel[1] in 1869. Twelve years later, Berthelot and Vieille[2] attempted to create detonations in different fuels

mixed with various oxidizers. Through the analysis of the velocities, the two confirmed the existence of detonations in gaseous mixtures. Following this discovery, true detonation research began rapidly accelerating. In 1883, Mallard and Le Chatlier[3] observed the Deflagration-to-Detonation Transition (DDT).

Following the observation made by the previously discussed authors, Chapman[4] in 1889 and Jouget[5] in 1904 began crafting theories regarding the mechanics of detonation waves. Chapman-Jouguet (CJ) theory models the detonation front as a shock wave propagating through space followed by an exothermic heat release. Both the shock wave and heat release are modeled as infinitely thin, and reactants turn into products across the shock. CJ theory is still used today to determine the presence of detonations based upon velocities. Zeldovich[6], von Neumann[7] and Doring[8], independently from each other, made the next big discovery in detonations during World War Two. Zeldovich, von Neumann and Doring (ZND) theory expands upon CJ theory to model the detonation as a shock wave followed by a reaction zone. The shock creates a pressure rise which compresses the gas enough to ignite the reactants, and the subsequent expansion of product gases provides the energy to continue the shock propagation. Both CJ theory and ZND theory are discussed in more detail in Section 2.3.

2.2   Structure of a Detonation Front

The diagram in Fig. 2.1 outlines the structure of a detonation front and serves to create a reference for terms used throughout the paper. Three shock waves exist in the detonation front: the Mach stem, the incident shock and the transverse shock. The points where the three shock waves meet are the triple points (A and B). The length between the triple points is the cell size (λ).
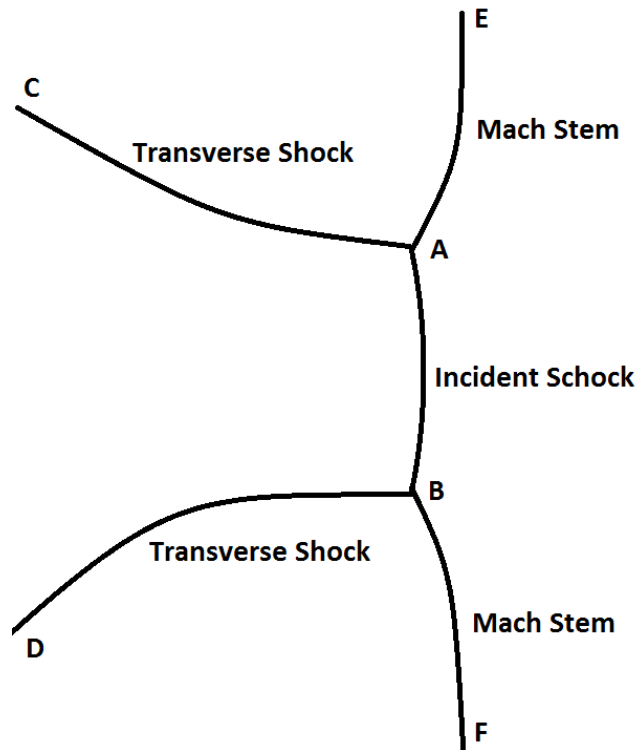
Figure 2.1. 2D cell structure of a detonation front

2.3 Detonation Mechanics

Falempin[9] describes that in a deflagration process the flame propagation is a function of the heat transfer from the reactive mixture to the fresh, unburned mixture. In other words, the energy released by the burning of fuel and air molecules initiates the burning of the unburned fuel and air in the surrounding area. The release of energy creates steep temperature gradients across the reaction front, resulting in the transport of heat and radical species from the reaction zone into the reactants ahead of the front. Lee[10] writes that due to the gradients a deflagration event is modeled as a diffusion wave, and therefore has velocity which is subsonic, and proportional to the square root of the diffusivity and reaction rate. As evidenced by the flickering of a candle or a Bunsen burner, deflagrations are inherently unstable due to varying interactions between the fuel, air and reaction front.

6

The instability of the burning process is also present when the fuel/air mixture is confined in a device such as a tube. This confinement coupled with the naturally occurring instability makes the reaction front even more turbulent and its propagation speed is increased. The boundary layer created along the wall also adds to the instability and when proper conditions are created, the flow abruptly transitions to detonation, as outlined by Lee[10]. More will be discussed on this transition later in Section 2.3.3.

The most notable differences between a detonation front and a deflagration front is the velocity at which the wave propagates, and the pressure rise created by the burning. As described by Soloukhin[11], a detonation wave is essentially a self-supporting shock wave in which a chemical reaction is continuously initiated by the adiabatic compression and heating of the gas in the shock front. The coupling of the shock wave and the combustion region is difficult to maintain, and often results in separation. Figure 2.2 presents a comparison of the velocity, Mach numbers, pressure, temperature and density ratios before and after a detonation wave passes through a medium. As seen in Fig. 2.2, detonation fronts produce a compression wave which increases both the pressure and the density of the gas. However, the pressure rise of a detonation event raises the temperature of the gas moreso than a deflagration event does. One more distinction between a detonation event and a deflagration event is the latter is modeled as a constant pressure process. Figure 2.2 shows the reason for this in that the typical pressure loss is minimal at approximately 0.98 of the pre-wave value.

With this foundational knowledge in mind, let us turn to a discussion of the CJ and ZND theories.

2.3.1 Chapman-Jouguet Theory

Chapman and Jouguet, independently from each other, created the first theory which modeled detonation waves and provided a means of solving for properties. Although CJ theory does not truly represent the physical characteristics of a detonation

Figure 2.2. Comparison of detonation and deflagration properties by Glassman[12]

front, the theory allows for a model of the fluid dynamics of the process. CJ theory models the detonation front as a planar shock wave traveling through a medium followed by the combustion front modeled by a heat addition, which occurs abruptly after the shock wave passes through the gas. This model is used to discover the global velocities of the flow, but runs under the assumptions of thermal and viscous limits being negligible, as described by Nettleton[13]. Figure 2.3 shows a sketch of the CJ model of a detonation front traveling through a gaseous mixture. The detonation front in Fig. 2.3 is stationary while, the properties of reactants denoted by the subscript (1) are moving to the left and the properties of the products are denoted by the subscript (2).
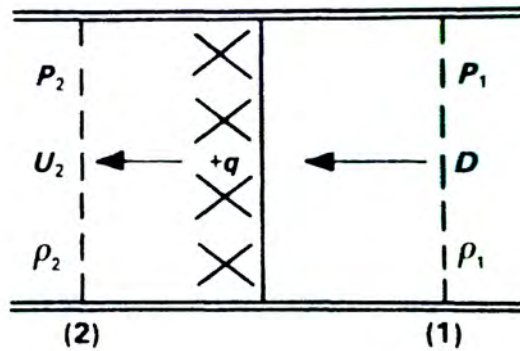
Figure 2.3. Sketch of CJ model of a detonation front by Glassman[12]

8

The CJ properties are found by locating the intersections of the Rayleigh line with the Hugoniot equation. Equation 2.1 describes the Rayleigh line, which gives the end states for mass flow traveling through a shock:

$$\dot{m}^2 = (u_1\rho_1)^2 = (u_2\rho_2)^2 = \frac{p_2 - p_1}{\frac{1}{\rho_1} - \frac{1}{\rho_2}} \tag{2.1}$$

The equation for the Hugoniot curve is a representation of the possible downstream states for a particular upstream state and is provided in Eqn. 2.2:

$$h_2 - (h_1 + q) = \frac{1}{2}(p_2 + p_1)(\frac{1}{\rho_1} - \frac{1}{\rho_2}) \tag{2.2}$$

Figure 2.4 shows the relationship between the two equations. The intersection between the Rayleigh line and the Hugoniot curve show the loci at which the detonation and deflagration can exist. The slope of the Rayleigh line represents the velocity of the particular front. There are two points where a detonation can exist for a particular velocity, and two points where a deflagration can exist for a particular velocity.
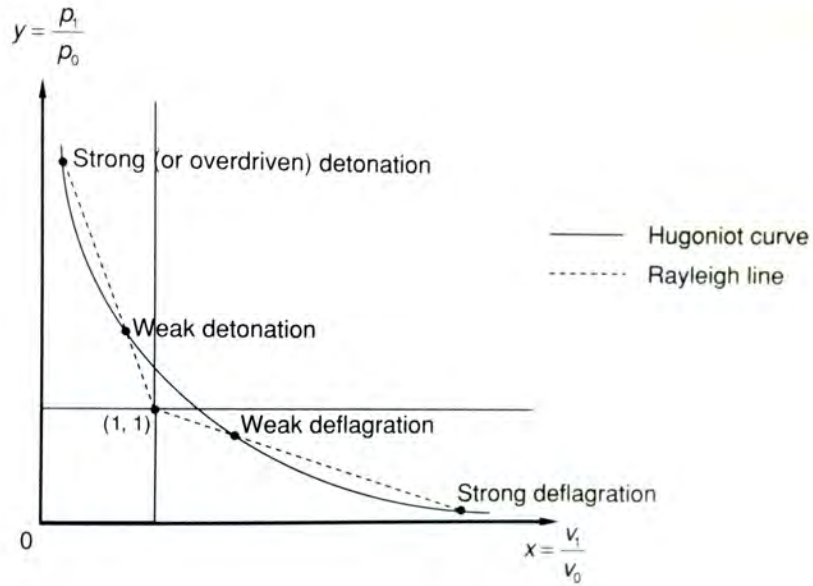
Figure 2.4. Rayleigh line and the Hugoniot curve from Lee[10]

Glassman[12] describes that at the CJ point in Fig. 2.5 the velocity of the detonation wave is equal to the speed of sound in the burned gases plus the mass velocity of the gases, and therefore rarefaction generated by the shock will not overtake the detonation. At the CJ solutions in Fig. 2.5, there is a minimum velocity for a detonation to occur, and a maximum velocity at which deflagration can occur. If the velocity decreases past the CJ point, then the Rayleigh line would no longer intersect the Hugoniot. Similarly the Rayleigh line would no longer intersect the Hugoniot for deflagration if the velocity increases.

Using the relationships from Eqn 2.1 and Eqn 2.2, the velocity and pressure for the detonation front is found at the CJ point. The most glaring problem with the CJ model is reaction rates are not infinite, and therefore the heat addition does not occur immediately at the plane of the detonation wave. Therefore, while the CJ model takes into account the
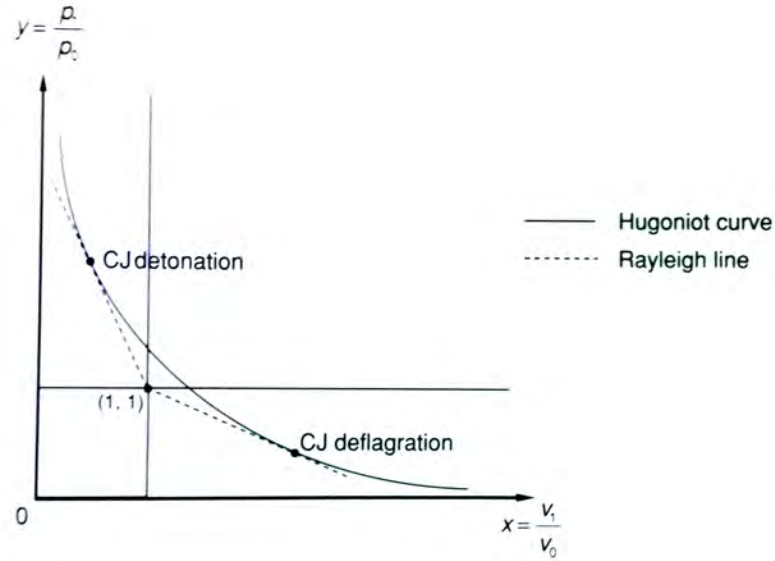
Figure 2.5. CJ solutions on the Hugoniot curve presented by Lee[10]

composition of the gases in the heat addition term, the theory does not take into account the time for the reaction of the particular fuel with an oxidizer.

2.3.2 ZND Theory

The ZND theory is an advancement over the CJ theory because ZND takes into account the chemical reaction rates behind the shock wave. Similar to CJ theory, ZND theory is one-dimensional and is able to provide solutions for the static parameters. ZND theory models the detonation wave as a planar shock which is followed by a heated and compressed gas. After the wave passes, the chemical reaction starts and the temperature rises, while the pressure and density fall until the CJ values are reached, as outlined by Glassman[12]. As seen in Fig. 2.6, pressure, temperature and density rise across the shock wave. Once the reaction begins behind the shock wave, the pressure and density decrease, while the temperature increases. The temperature increase is due to the release of heat from the reaction.

ZND theory asserts the existence of a pressure rise, which is necessary to get the
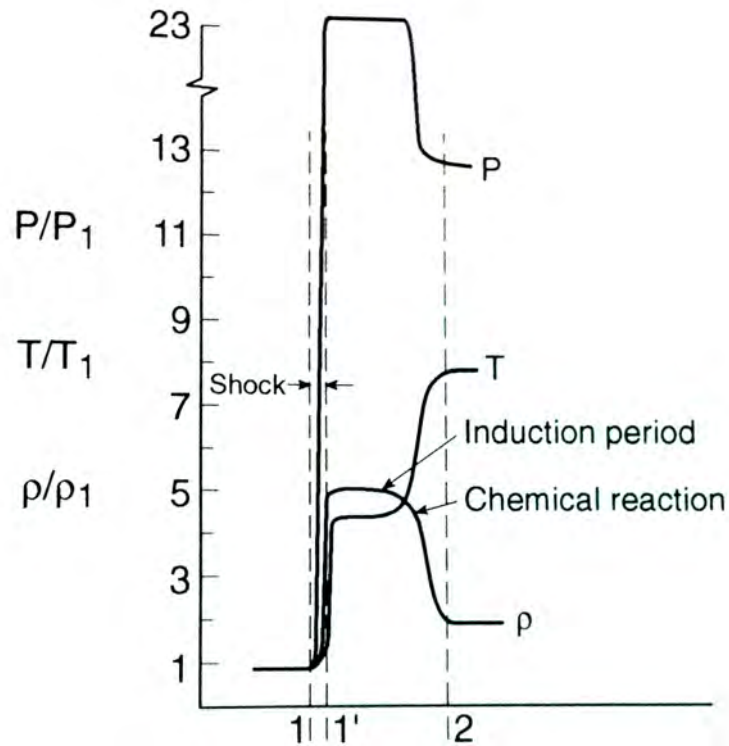
Figure 2.6. Behavior of physical properties according to ZND theory created by Glassman[12]

reaction started in order to have a self-sustaining detonation wave. Figure 2.6 shows that the pressure rise across the shock (23 on y-axis) is much greater than the CJ pressure (13 on y-axis). This evidence suggests that although the pressure rise found from CJ theory might not be enough to initiate a reaction in a particular mixture, the pressure rise across the shock could provide the necessary compression.

2.3.3 Deflagration to Detonation Transition

Direct initiation of a PDE requires a high-energy spark in an explosive mixture, which results in an instant detonation front. Direct initiation is not practical for aerospace applications due to the large amount of energy required each time the detonation starts in the PDE tube. A typical PDE operates on the order of 30-50 Hz, and if used in flight,

would require several hundred thousand detonations; therefore, a low-energy spark is a more efficient means to form the detonation front. A low-energy spark creates a deflagration event, which will eventually transition to a detonation front when conditions permit.

Soloukhin[11] describes the mechanism of the transition from deflagration to detonation as being due to strong distortions of the flame. The turbulence of the flame results in individual pockets of unburned mixture, which are surrounded by burned expanding gases. The expansion of the burned gas provides localized compressions and results in an explosion. In order for the transition to occur in a closed tube, the laminar flame front must travel a certain distance before the transition occurs. Soloukhin[11] cites several shock tube experiments that place the transition distance at approximately 30 to 70 tube diameters before DDT occurs. The reason for the long tube length is due to the need for a boundary layer to form in the tube. Solukhin[11] asserts that the unsteadiness in the flow leads to the localized explosions (hot spots) which facilitate the detonation formation. For larger diameter tubes, waiting for the boundary layer to form is impractical due to long the long tube lengths required to form the boundary layer.

2.3.3.1   Schelkin Spiral

In 1954 Schelkin[14] attempted to promote earlier DDT by placing a spiral device in the tube, as seen in Fig. 2.7. Inserting a spiral into the tube increased unsteadiness and created localized explosion within the flow. After adding the spiral to the tube Schelkin[14] observed quasi-steady detonations propagating at as low as 30% of normal CJ velocities. This phenomenon occurs because shock waves reflect off of the spiral, which leads to the creation of hot spots.
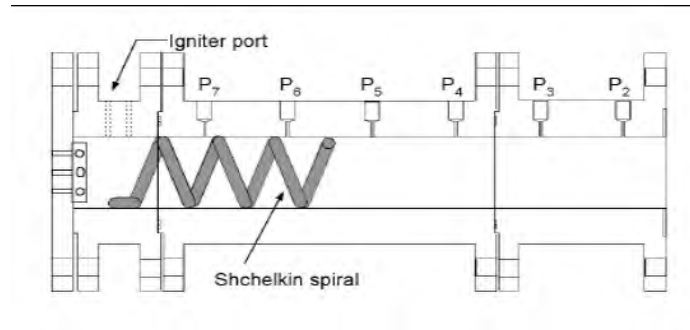
Figure 2.7. Schelkin spiral in a detonation tube from an experiment conducted by Lu[15]

2.3.4   Diffraction of Detonation Waves

Three scenarios are of primary interest in studying the diffraction of detonation waves; how the detonation wave behaves when striking an isolated wall; when the wave is confined and entering a convergent or divergent section; and when the wave is entering open space from a confined section. In detonation diffraction (and similarly in non-reactive shock diffraction) Nettleton[13] states there exists a wedge angle θ_{crit} which determines whether or not the shock will undergo Mach or regular reflection. In Mach reflection the incident front will form a Mach stem with the wall, as can be seen in Fig. 2.8. In regular reflection, the reflected wave is parallel to the wall (See Fig. 2.9). In the latter instance, point O would move down to the wall.

Nettleton[13] asserts that the difference between Mach and regular reflection stems from the need of the flow to become parallel with the wall. At larger angles the flow is rendered parallel by the incident wave (line OR). In Mach reflection, a Mach stem (line TM) forms to turn the flow to be parallel to the wall, as seen in Fig. 2.8. Finally, the reflected wave (line TR), turns the flow to be parallel to the ground plane.
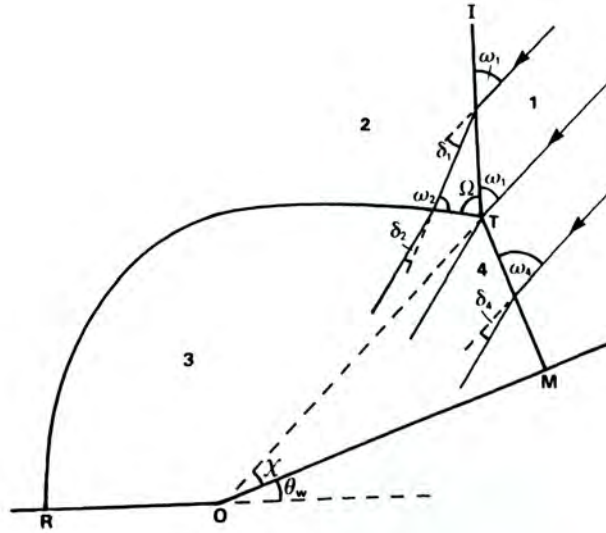
Figure 2.8. Shock wave undergoing Mach reflection diagrammed by Nettleton[13]
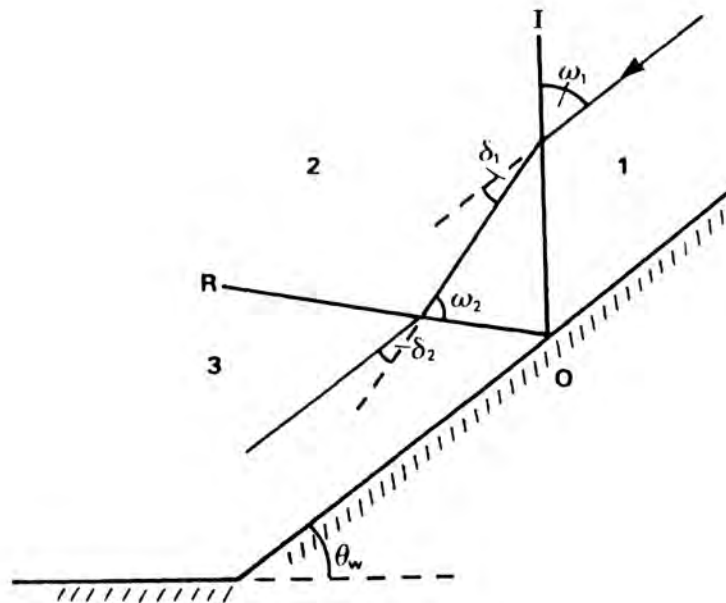
Figure 2.9. Shock wave undergoing regular reflection diagrammed by Nettleton[13]

Regular, non-reactive shock theory provides a basic means to get the pressure rise across the various shock fronts. Equation 2.3 is used to get the pressure rise across the

15

incident wave:

$$\frac{p_2}{p_1} = \frac{2\gamma M^2 \sin^2 \omega_1 - (\gamma - 1)}{\gamma + 1} \qquad (2.3)$$

The limitations from Eqn 2.3 stem from its inability to take into account the energy released by the reaction front of the detonation wave and the change in γ on either side of the detonation wave.

For the Mach stem, which is traveling directly into the flow, Eqn. 2.4 is used to solve for the pressure rise. In Eqn 2.4 D_{CJ} is the CJ velocity of the wave and u_2 is the velocity of the flow. Nettleton[13] uses the subscripts 1 and 2 to represent the gas in front of and behind the detonation front, respectively.

$$D_{CJ}^2 + \frac{2\gamma_1}{\gamma_1 - 1}\frac{p_1}{\rho_1}(1 + q) = u_2^2 + \frac{2\gamma_2}{\gamma_2 - 1}\frac{p_2}{\rho_2} \qquad (2.4)$$

A more detailed derivation of these two equations is found in Nettleton's *Gaseous Detonations*[13]. If de-coupling of the reaction front and the shock has happened, the normal shock theory is sufficient to help determine if the pressure ratio of the front will be enough to re-ignite the shock on a wedge.

2.3.5 Area Expansion

In 1957, Zeldovich *et al.*[16] tested the expansion of detonation waves into an unconfined space from tubes of different diameter. They determined the existence of a critical tube diameter wherein diameters below the critical width resulted in de-coupling of the detonation front, while diameters above the critical width allowed for successful re-initiation.

Figure 2.10 shows a set of still frames from the supercritical tube diameter taken by Soloukhin[11]. The frame at $9\mu s$ shows the front of the wave (to the right) as being a detonation front, while the back part (to the left) is a smooth line. The difference in shape is due to large expansion waves off the corner of the tube which quench the detonation

16

front as it exits. Although not shown, eventually the front detonation wave will propagate and re-initiate the back.
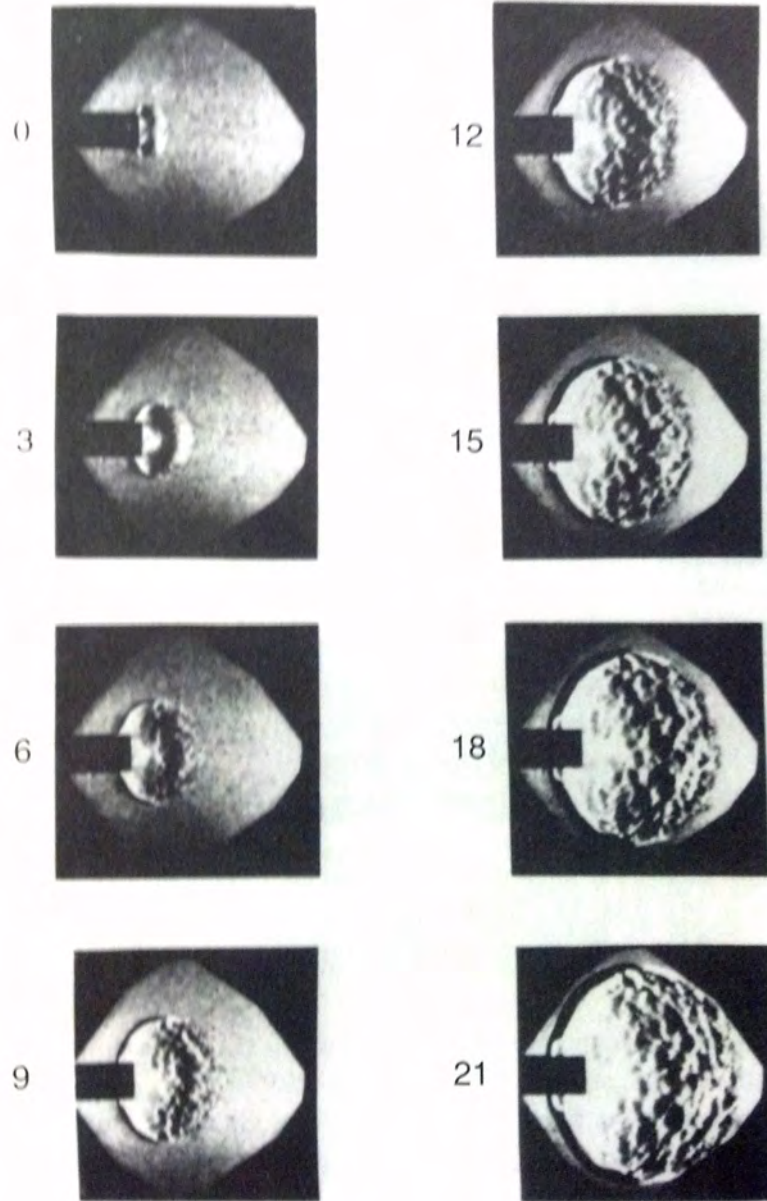
Figure 2.10. Detonation wave exiting a supercritical tube diameter, images taken by Soloukhin[11]

17

Figure 2.11 shows a set of still frames from the critical tube diameter case. In frame (b) the detonation front has begun to re-form after initially decoupling. The "bubble" then expands and eventually engulfs the decoupled region near the tube exit in frames (c) and (d). At the end of the frames almost the entire front has re-initiated in the open space.
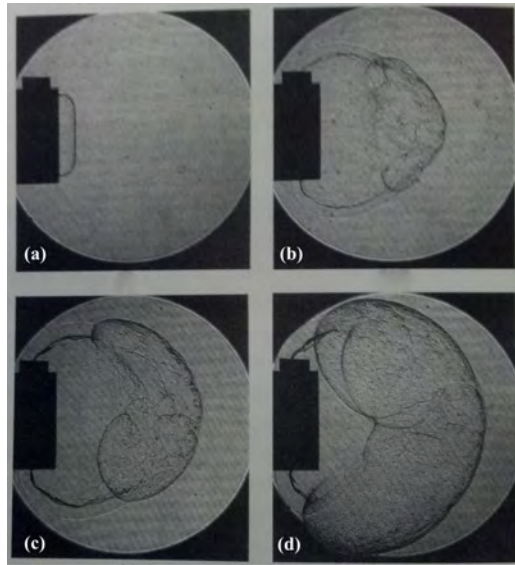
Figure 2.11. Detonation wave exiting a critical tube diameter, images taken by Schultz *et. al*[17]

Figure 2.12 shows a plot of the critical diameter as a function of the stoichiometric fraction of various fuel and oxidizer mixtures. Of primary interest in Fig. 2.12 is the relationship between Hydrogen and Oxygen, as those were the primary fuel and oxidizer used throughout the thesis experiments. Figure 2.12 shows the critical diameter at its lowest point of around 20 mm at a stoichiometric value equal to 1. As the stoichiometric fraction is reduced (air is increased) the critical diameter is increased. The same relationship is visible for an increase in the amount of fuel in the mixture. The relationship between stoichiometric fraction and critical diameter is intuitive, as a perfect balance between fuel and air will reduce the need for a larger detonation wave to make the

transfer from confined to unconfined space.
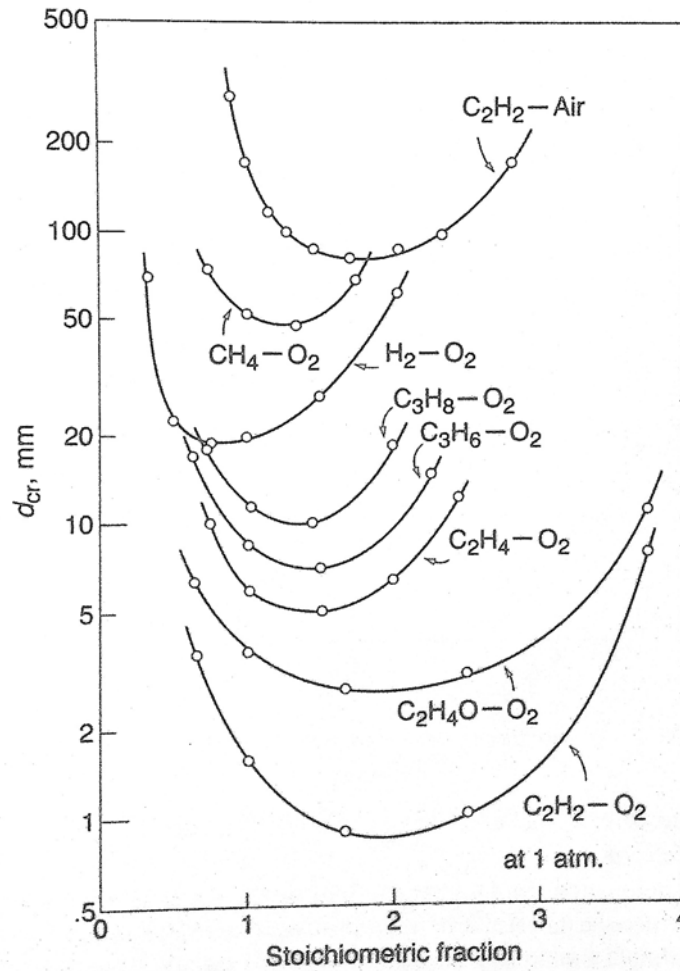
Figure 2.12. Critical diameters for various fuels at different equivalence ratios found be Matsui[18]

In 1964, Soloukhin[11] proposed a relationship between the critical tube diameter and the cell width of the detonation wave. Equation 2.5 shows the relationship as:

$$d_c = 13\,\lambda \qquad\qquad (2.5)$$

Knystautas *et. al*[19] validated the 13 λ relationship in their study comparing critical

19

diameters derived experimentally to those derived from the 13 λ correlation. Figure 2.13 shows the critical diameters for various fuels found as a function of equivalence ratio. The line values are the critical diameters as found with the 13 λ correlation, while the shapes are the values found experimentally. In Fig. 2.13 it is important to note that for Hydrogen (the hexagon shape) the validity of the correlation is upheld by the experimental results, as this is the fuel used throughout the experimentation section.
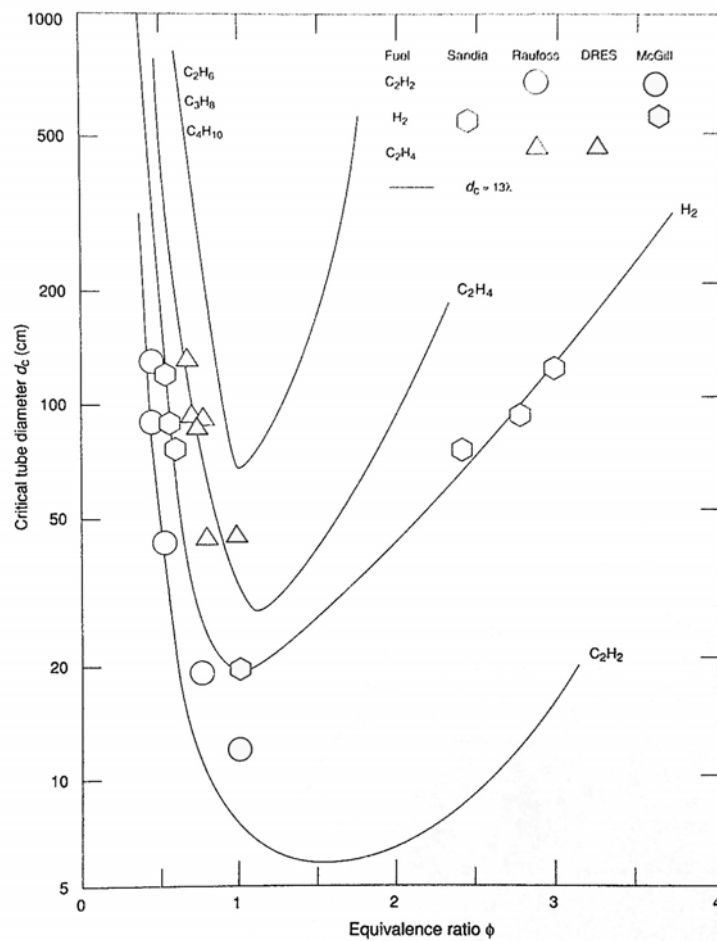
Figure 2.13. Comparison of the 13 λ correlation to actual critical diameters as found by Knystautas[19]

2.4 Rotating Detonation Engines

A rotating detonation engine behaves as if there is an infinite tube length present for the detonation to propagate in. In a RDE, the detonation wave is initiated by a pre-detonator, which then enters a radial chamber. The wave propagates around the circumference of the circle as long as long as fuel and air is provided to sustain the detonation.

2.4.1 Cycle

Similar to a PDE, the RDE operates on a fill, fire and purge cycle, but does so at a much higher rate. Figure 2.14 shows a sketch of a detonation wave traveling clockwise around a curved channel, from a plan view. In a RDE the fuel and air enter from separate nozzles at the bottom of the channel; they are not typically pre-mixed. Soloukhin[11] shows in Fig. 2.14 the triple point structure, wherein the front from point B to point C compresses the mixture, and combustion occurs behind the front from point C to point D. As the detonation wave travels around the channel, the burned gas is expelled out of the top (opposite to the injectors) and new mixture is filled in from the bottom. Typically RDE's operate at a much higher frequency than PDEs in the range of 2-3 kHz.
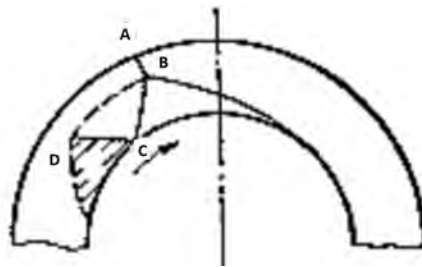
Figure 2.14. A sketch of an RDE[11]

21

2.4.2   Benefits

There are several benefits to operating with a RDE as opposed to a PDE. Firstly, the RDE is continuous and does not require initiation for every cycle. Whereas the PDE needs to be initiated for each cycle, the RDE wave is self-sustaining as long as fuel and air are provided, and assuming the device does not melt. The sustainment can save money on both the energy required for each spark and the need for aircraft to carry highly reactive gas mixtures for the pre-detonator, depending on the initiation scheme.

The second benefit is the high cycle count of the RDE. A typical PDE engine operates between 30-70 Hz, while a RDE operates at around 2-3 kHz. The difference in cycle rates is due to the PDE operating with valves, while the RDE has a constant fill and purge. The PDE requires valves for filling the detonation with the fuel/air mixture and for filling the tube with cold air used to purge the reactants. The RDE has a constant fill from the bottom of the circular channel. As the detonation travels around the channel, the fuel and air fill from the bottom and the reactants flow out the top. The high cycle count allows for the integration of downstream components which will not be required to deal with the pulsation present in a PDE, which can introduce fatigue and reduce life expectancy. The RDEs high cycle count produces flow similar to that of constant gas turbine burner.

The third benefit is the compact nature of the RDE. RDEs have been made with diameters as small as 75 mm. Typical PDEs require long lengths of tube in order to produce the DDT. This characteristic makes PDEs unsuitable for integration into existing engines. The smaller and more versatile RDEs can more easily be installed to fit into current spaces operated by traditional burners.

2.4.3   Limitations

Kailasanath[20] writes that one obstacle present in RDEs is the heat transfer to the walls of the chamber which is caused by the high cycle rate. Unlike the PDE, the RDE is not cooled after each detonation front by colder reactants due to the continuous detonation

in the RDE chamber. Another problem is the fuel and air are not premixed and enter the channel at different points. Falempin[9] believes the lack of pre-mixing the fuel and oxidizer, and the small times between detonations, can lead to less than ideal mixing, which can alter the detonation characteristics. The fresh gases could also mix with the products leaving the channel, and cause some of the fuel not to react.

2.4.4   Previous Rotating Detonation Engine Work

Shank[21] revealed the need for further testing of RDE initiation schemes during previous work at the Detonation Engine Research Facility (DERF) at Wright Patterson Air Force Base (WPAFB). Shank[21] ran a 150 mm diameter RDE, which had a 7.5 mm wide channel. This RDE runs on hydrogen and air at various mass flows and equivalence ratios. Researchers at the DERF created the 150 mm RDE in a modular manner in order to easily interchange different components. The RDE is shown in Fig. 2.15.
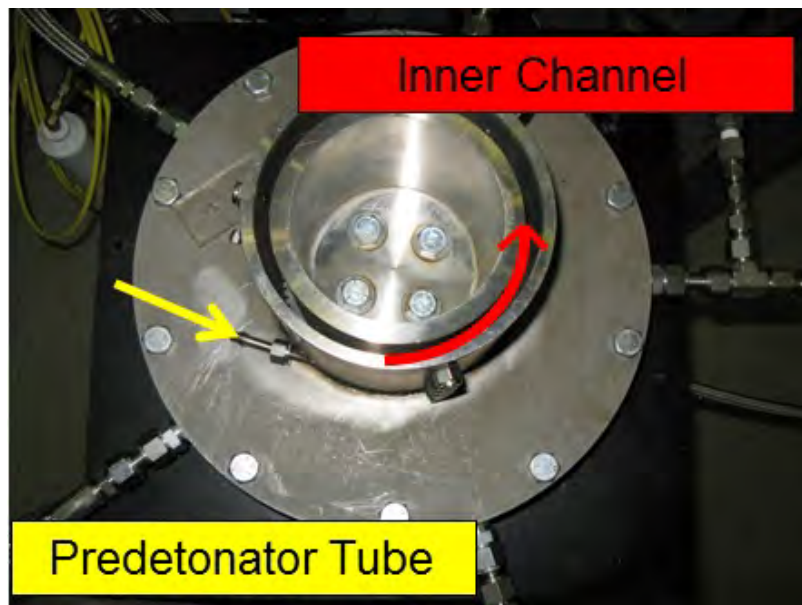
Figure 2.15. Plan view of the 150 mm RDE experiment on by Shank[21]

2.4.4.1 Initiation

A pre-detonator connected tangentially to the RDE channel starts the detonation wave. The pre-detonator is made of stainless steel, is 63.5 mm long and has a 6.35 mm diameter. It operates with hydrogen as the fuel and oxygen as the oxidizer. The pre-detonator enters the RDE channel at 25 mm above the base plate. The setup of the pre-detonator is shown in Fig. 2.16. Figure 2.16 shows a plan view of the pre-detonator resting on the RDE baseplate. The hydrogen and oxygen supplies enter directly perpendicular to the spark plug and are oriented facing each other to promote mixing. The detonation wave travels around the RDE channel after being started in the pre-detonator tube.
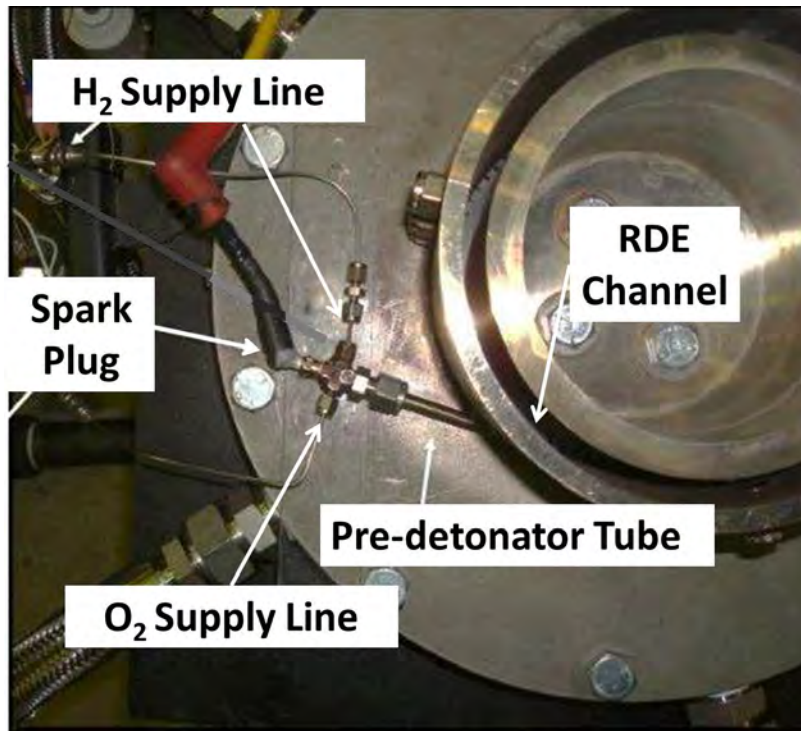
Figure 2.16. Plan view of pre-detonator installed on 150 mm RDE tested by Shank[21]

2.4.4.2   Problem Modes

In previous experiments the RDE ran successfully. Shank[21] determined the best operating conditions occurred between an equivalence ratio of 0.9 and 1.3, with a mass flow between 160 and 200 *lbm/min*, as seen in Fig. 2.17. Figure 2.17 has the equivalence ratio of the hydrogen/air mixture in the channel on the x-axis. The y-axis has the mass flow rate from the hydrogen and air supplies in the RDE channel. Successful runs of the RDE had a detonation wave travel once around the channel and are represented by the red marks. A deflagration wave or a problem mode represent unsuccessful operation and are represented by the blue marks. Detonations are validated by high speed video and pressure data from ports located around the circumference of the RDE. Using these two measurement techniques and comparing to CJ velocities helps to determine if a detonation or deflagration wave is occurring in the chamber.
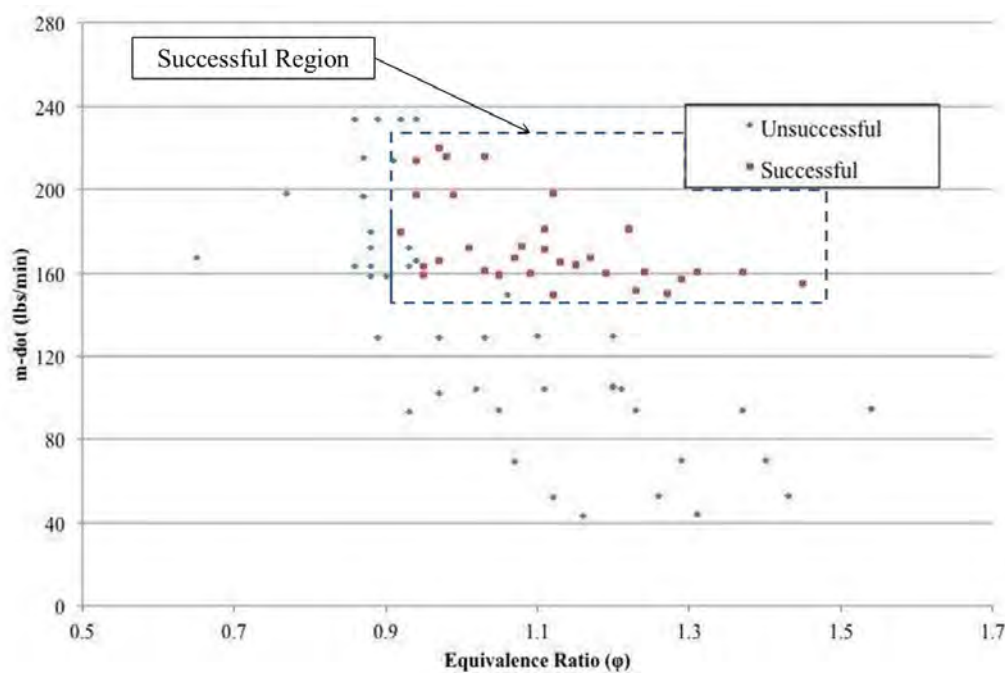
Figure 2.17. Operational space for 150 mm diameter RDE as reported by Shank[21]

Shank[21] outlined three different modes present during operation of the RDE. In the rotation mode the detonation wave successfully travels around the inner channel of the RDE in either direction. In one problem mode, the detonation wave travels counter-clockwise around the RDE, but eventually reverses direction and travels around the chamber clockwise (Fig. 2.18). The counter-rotation also occurs upon initiation, wherein the wave travels in the direction opposite than that than expected or desired. Figure 2.18 shows the detonation wave (bright spot) traveling counter-clockwise in Frames 1 through 4, before stopping in Frame 5, and then reversing for Frames 6 through 10.
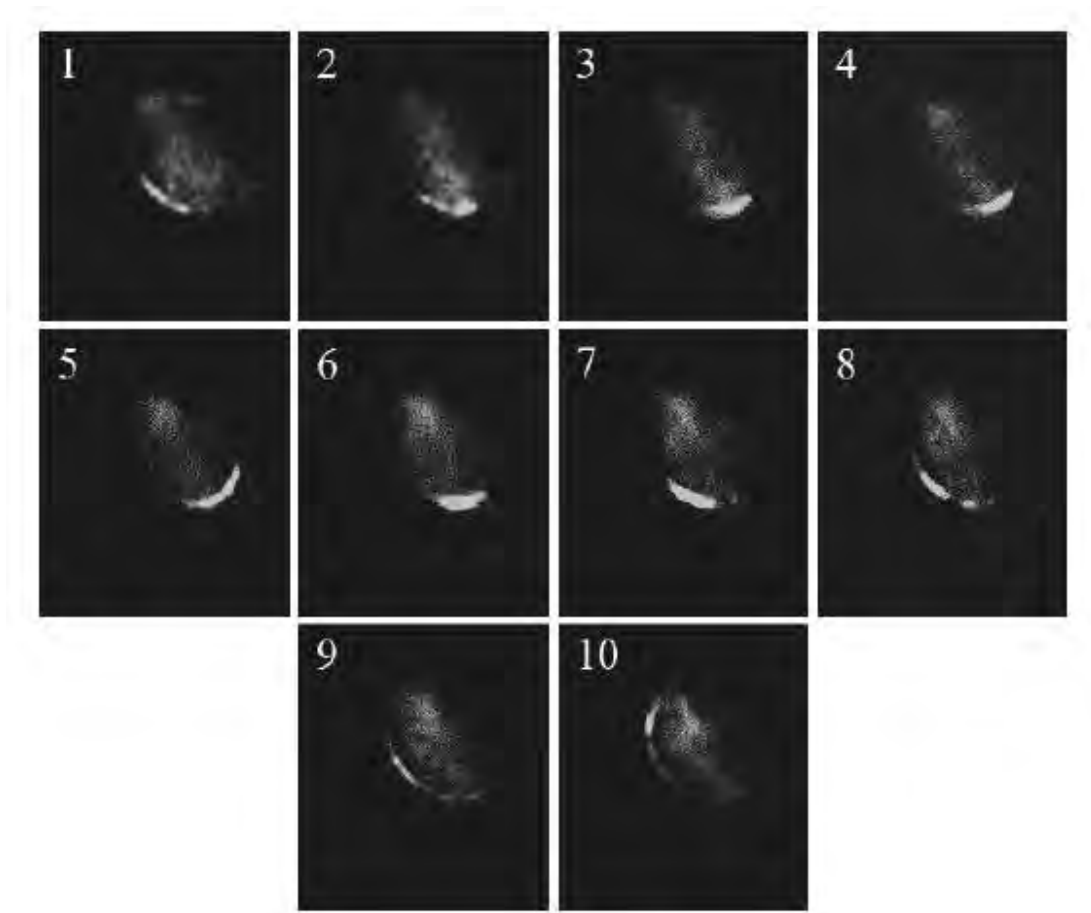
Figure 2.18. Plan view of 150 mm RDE exhibiting the reversal mode of operation, image taken by Shank[21]

The second problem mode occurs during start up and normal operation, wherein the detonation wave bifurcates. After splitting, the two detonation fronts will travel around the chamber in opposite directions (Fig. 2.19). In some instances the detonation waves re-couple and continue after colliding. In other instances two detonation fronts travel back around the chamber following the collision.

Figure 2.19. Plan view of 150 mm RDE exhibiting the bifurcation mode of operation, images taken by Shank[21]

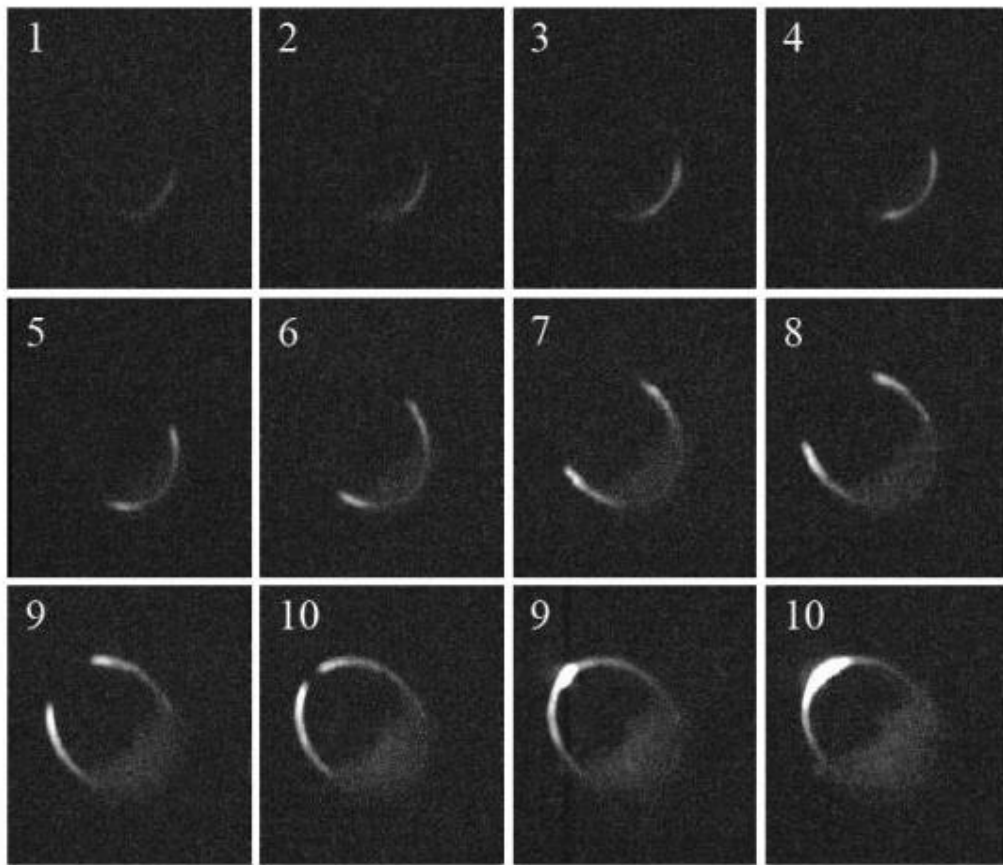Shank[21] hypothesized that the detonation wave from the pre-detonator does not successfully transition into the RDE channel. This poor transition to the channel results in a randomness to the direction of re-initiation.

27

2.5 RDE Initiation Schemes

2.5.1 Blasting Wire

Le Naour *et al.*[22] conducted work on a 100 mm RDE. The engine built by the team has a few differences from the 150 mm RDE manufactured by the DERF. This teams RDE utilizes a different initiation scheme and fuel/oxidizer injection set-up to the 150 mm RDE. The fuel and oxidizer are injected from the bottom of the channel, but both are aligned axially to the chamber. This injection scheme is different from Shank's[21] RDE because the oxidizer does not enter the chamber perpendicular to the flow of the fuel. Le Naour's[22] published findings speak more about their experiments and testing than the initiation scheme, but he mentions the RDE is started through the use of a blasting wire. Instead of using a low energy spark like Shank[21], the energy from the explosion is roughly 10 J. After the blasting wire ignites the detonation wave, it travels into the RDE channel. The authors do not go into detail regarding the success of achieving detonations, but the feasibility of the system can be analyzed. An explosive wire device is typically used in explosives for detonating charges. In order to get the reaction started, the system requires a large surge in energy which provides the explosive with the necessary energy to begin the reaction. Although good for testing on ground, the device would require a large power source to be carried on any aircraft which utilized the blasting wire setup. Consequently an explosive wire device is not ideal for use in future RDE applications.

2.5.2 Swirled Injection RDE

A more novel approach to RDE initiation used by Braun *et al.*[23] used no pre-detonator at all. Instead of using a pre-detonator, Braun oriented a spark plug flush with the outer wall of the RDE channel. Using a set timing schedule on the injection valves, Braun provided fuel and air in the direction the detonation wave would travel, as outlined in Fig. 2.20. The swirl injection method ensures the detonation wave will not travel clockwise due to there being no fuel or oxidizer to propagate in. Braun[23] tested

two engines. The first mixed the fuel and air in the detonation chamber, while the second pre-mixed the fuel and air before injecting it into the channel. The latter set-up also contained a water jacket for cooling the RDE during operation.
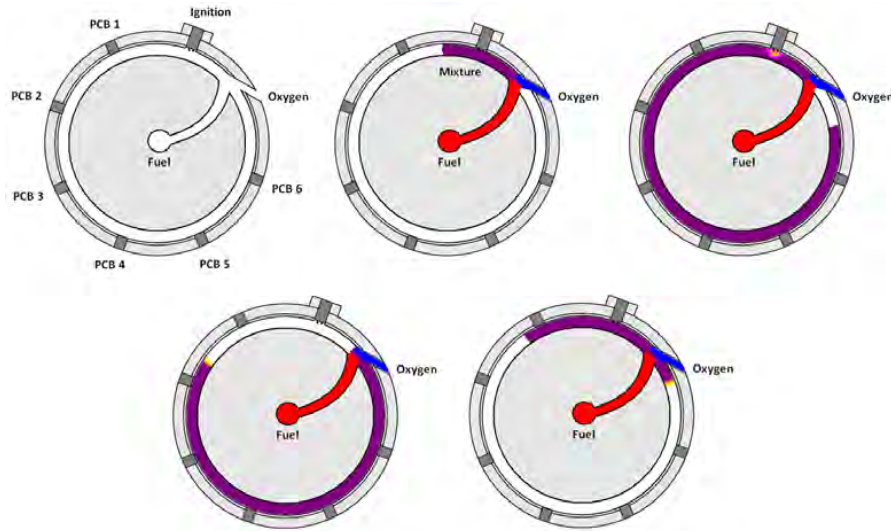
Figure 2.20. Initiation scheme of an RDE with swirl injectors created by Braun[23]

There is no data provided on the reliability of the swirl injection used by Braun[23]. In his thesis, Shank[21] hypothesized the detonation wave reversed direction in the 150 mm RDE due to the pressure transducer and pre-detonator injection sites. Adding more geometric features to the channel provides an increased number of reflection points that remove energy from the detonation front. If enough energy is removed, the detonation will decouple and could re-initiate in either direction. A separate but equally important problem is that leaving the spark plug in the flow could lead to the exposed portion melting and would result in having to replace the plug with longer runs. Automotive spark plugs can withstand detonations in PDEs, but the higher cycle rate of the RDE could create a dangerous environment.

2.6 Diffraction of Detonation Waves at a Convex Corner

Bartlma and Schroder[24] showed the effect of cell size on the diffraction of a detonation wave at a convex corner. Figure 2.21 and Fig. 2.22 provide some understanding as to how the detonation wave will travel from a narrow pre-detonator tube into the unconfined channel of the RDE. Fig. 2.21 shows a detonation wave approaching a 135° corner, exiting a tube diameter of greater than 13 cell widths. After the detonation wave travels around the corner into the open space, the shock wave and the combustion front are able to remain attached.

Figure 2.21. Detonation wave approaching a 135° corner (8.1% propane, 40.3% oxygen and 51.6% argon), images taken by Bartlma and Schroder[24]

Fig. 2.22 shows a detonation wave approaching a 135° corner, with a tube diameter of less than 10 cells. Although the geometry is the same, the concentration of propane has been reduced subsequently increasing the cell size. Once the detonation wave enters the open space, the shock wave separates from the combustion front almost immediately.
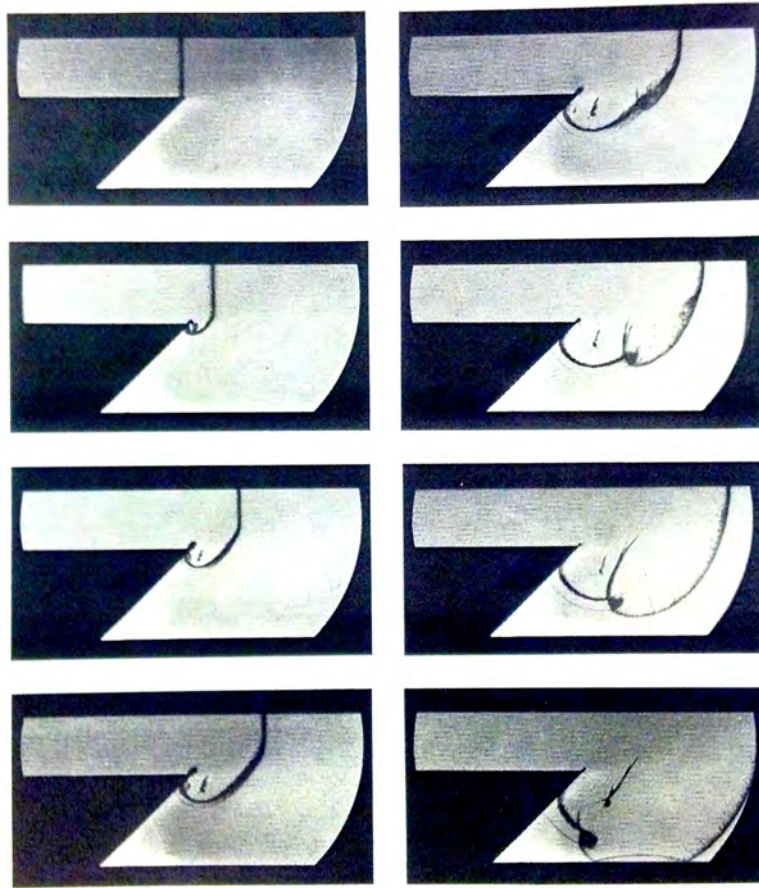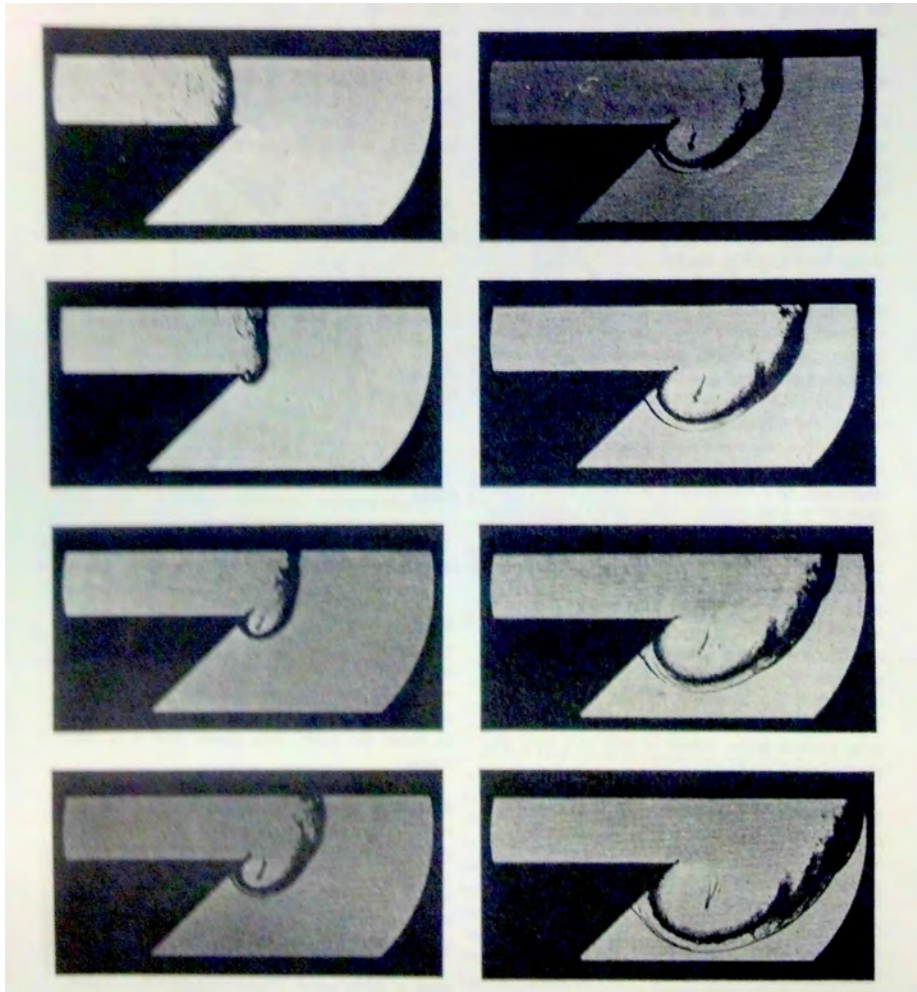

Figure 2.22. Detonation wave approaching a 135° corner (6.2% propane, 31.2% oxygen and 62.6% argon), images taken by Bartlma and Schroder[24]

2.7   Detonation Re-initiation

Stevens *et al.*[25] tested the ability of geometric shapes to re-ignite decoupled detonation waves. Stevens connected a test section with polycarbonate windows to the PDE. A coupled detonation wave traveled into the test section between points (0, -40) and (0, 0) in Fig. 2.23. As indicated by the red areas, the detonation wave decoupled before striking the wedge at point (169, 40). This research tested various geometries downstream of the decoupling to see whether or not the detonation could be re-initiated, the wedge is located in the upper right corner in Fig. 2.23 and Fig. 2.24. Of primary interest is the 45° wedge placed 169 mm downstream from the left hand wall, as this was tested with a pre-detonator in Sec. 4.4. As seen in Fig. 2.23, the wave first enters coupled at (0, -40), but de-couples at (150, 40) of the test section as denoted by the red. The wave travels left to right in Fig. 2.23, and re-couples approximately halfway up the wedge at (200, 40). Figure 2.24 shows the Mach number to be around 3.5 when the wave strikes the wedge. Stevens[25] reported a 45° wedge, coupled with a wave speed of Mach 3.5 resulted in re-initiation 44% of the time.

Figure 2.23. Separation distance between the shock wave and combustion front with wedge located 169 mm downstream created by Stevens[25]

Figure 2.24. Shock wave Mach numbers striking a 45° wedge located 169 mm downstream created by Stevens[25]

Stevens'[25] work provides an understanding as to the exit velocities needed for the shock wave to re-initiate the detonation. Section 4.4 reports on results of similar wedges place into the flow immediately after the pre-detonator. The wedges were placed in the simulated RDE channel in order to re-initiate the wave after it decoupled leaving the pre-detonator. Furthermore when the velocities are increased to Mach 5 (Fig. 2.26), the detonation front remains coupled (Fig. 2.25).
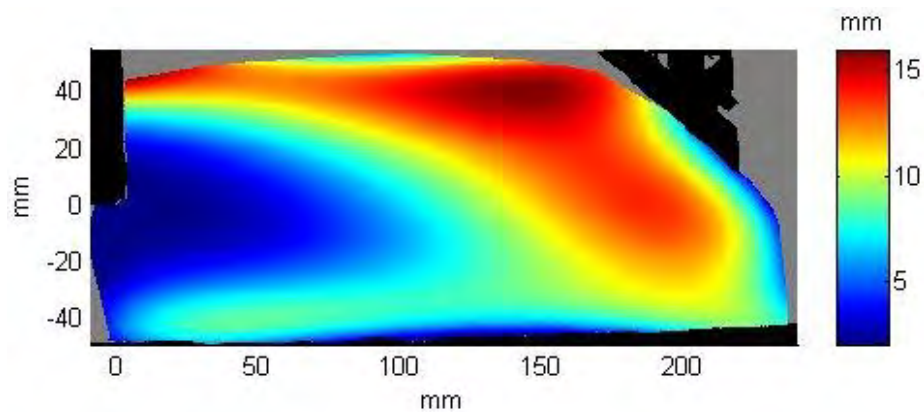

Figure 2.25. Separation distance between the shock wave and combustion front with wedge located 84.7 mm downstream created by Stevens[25]

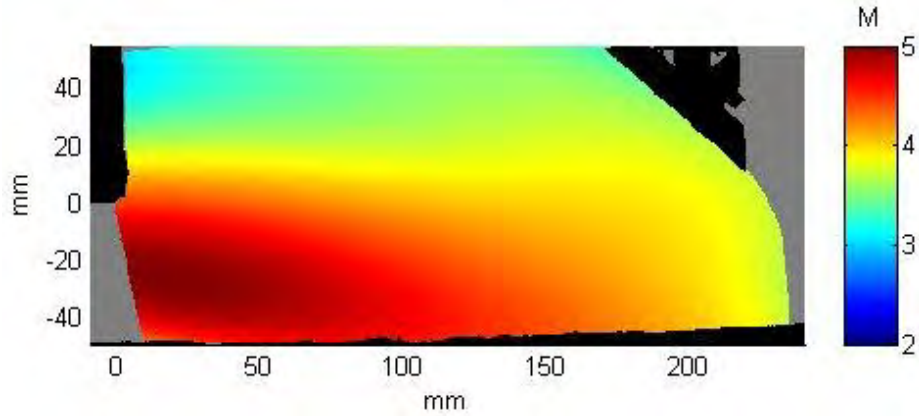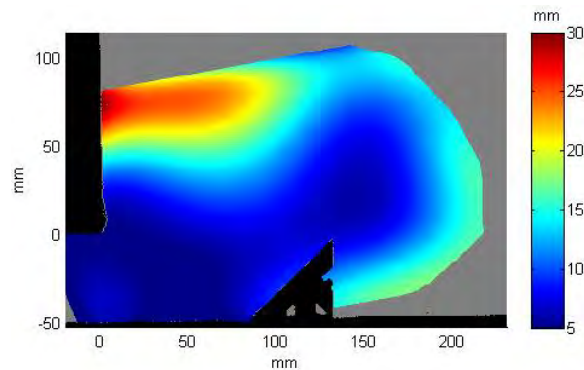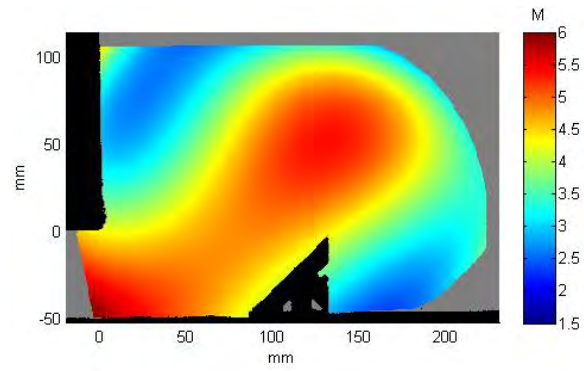Figure 2.26. Shock wave Mach numbers striking a 45° wedge located 84.7 mm downstream created by Stevens[25]

III. Experimental Facility and Design Methodology

All tests were conducted at the DERF located in Building 71A, D Bay, at Wright-Patterson AFB, OH. The DERF is run by the Air Force Research Laboratory Aerospace Systems Directorate, Turbine Engine Division, Combustion Branch(AFRL/RQTC). Originally built as an engine test cell for engines with up to 60,000 lbf of thrust, the bay is 21,200 m^3 and contains both pulse detonation engines and rotating detonation engines. A control room is located alongside the test cell, and is separated by a 2 ft wide concrete wall.

LabVIEW software regulates the air and fuel flow to the engine during operation. A high speed camera connected to the control room via an ethernet cable provided the videos for all tests. Work for this thesis was conducted using the PDE setup designed by Schauer *et. al*[27] and a standalone pre-detonator.

The test rig simulates the RDE channel, while allowing for flow visualization. Similar to the RDE which confines the detonation between the inner and outer body, the test set-up confines the detonation between the two windows. The space between the inner and outer bodies of the 150 mm RDE is 7.62 mm and the space between the two windows on the test setup is 6.35 mm. The two are different due to modifying a previously built test rig rather than building from scratch. The top of the RDE is open to air and allows for the exhaust gases to escape. While the test set-up does not have an open top (in order to contain the fill gases), the top part is located at 23 cm above the pre-detonator exit. Placing the top steel plate at 23 cm allows for the detonation to exit the pre-detonator and travel down the channel before interacting with the top plate. Furthermore the pre-detonator is located at 25 mm above the bottom plate, which is the same height as the RDE pre-detonator above the base plate.

Figure 3.1 shows a sketch of a plan view of the RDE and the test section. The red

lines are represent the side confinements, while the blue line represents the pre-detonator.

The 22° between the test rig pre-detonator and window matches the angle produced by the

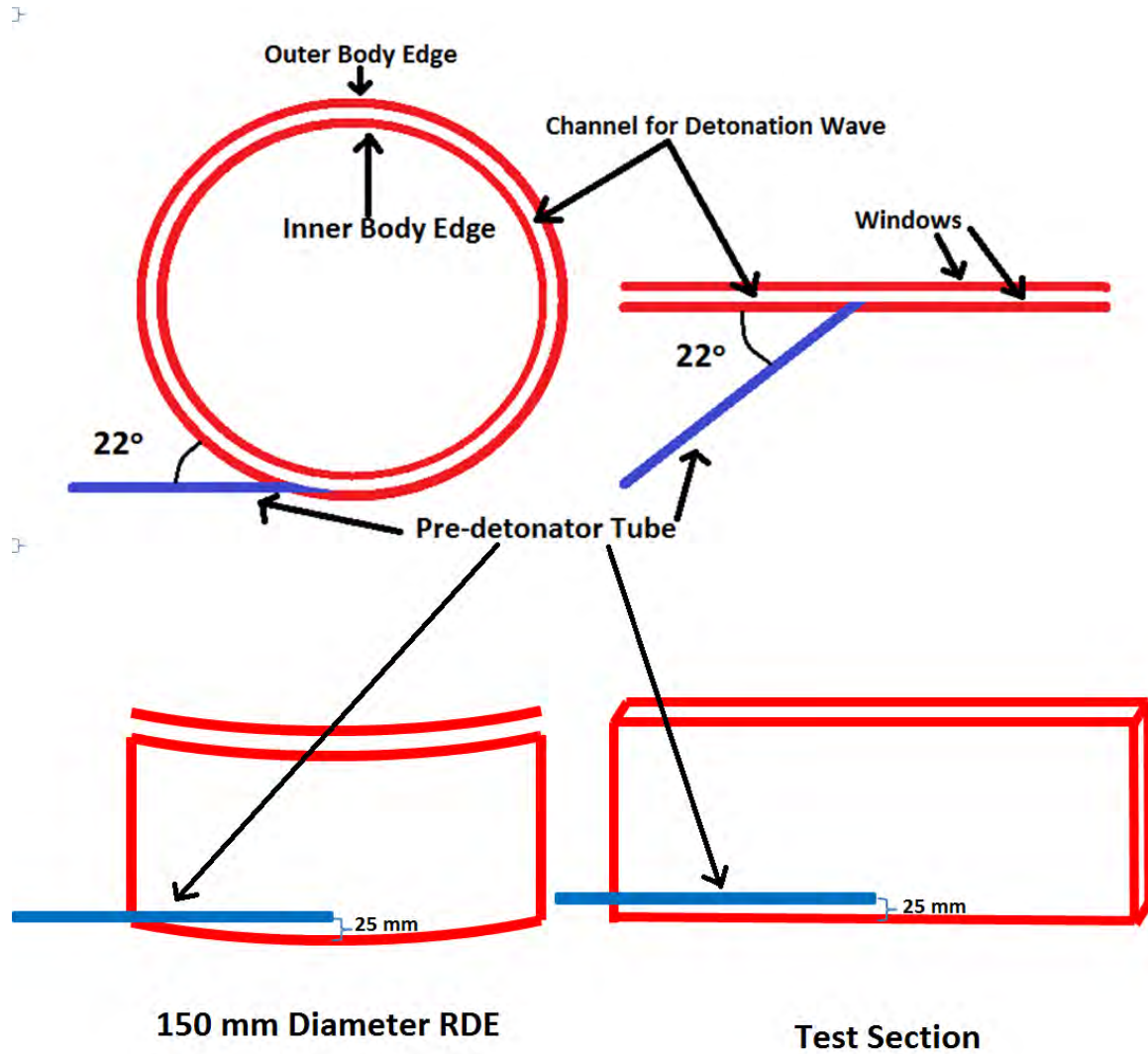circumference of the 150 mm RDE and the pre-detonator (Fig. 3.1).

Figure 3.1. Comparison sketch of 150 mm RDE (Left) and test section (Right)

The test rig possesses limitations in modeling the RDE initiation scheme that bear

brief discussion. Firstly, there is no curvature in the simulated channel. The lack of

curvature does not provide a significant issue, since focus of the research is on how the detonation wave moves from the pre-detonator into the narrow channel. This is the first research that shows the behavior of a detonation wave traveling from a narrow circular channel angled into a rectangular cross section channel; the transition is an environment unique to the RDE, and as such needs to be studied to understand initiation. Another limitation to the test set-up is the fuel and oxidizer injectors in the base plate. Adding the injector ports to future studies would be necessary to fully understand DDT in the RDE, but adds a lot of complexity to the design of the test-rig.

3.1 Pulse Detonation Engine

The PDE used in the DERF is built around a General Motors Quad 4 cylinder head. The PDE control system requires the tube and test section volume to be inputted to calibrate the fuel/air fill. The test section and tube volume for the test section is approximately 3,441 cm^3. The intake valves on the engine head fill the detonation tube with a pre-mixed fuel/air gas mixture. The exhaust valves flow opposite to those of a traditional car engine and fill with cold air to purge the product gases, while simultaneously cooling the tube. The PDE operates on a fill, fire, purge cycle, but for this testing the spark on the PDE was not fired. Each of the three sequences are approximately 33 ms for a standard run, adding up to a total cycle time of 100 ms. The control system outputs a voltage signal every 100 ms, which triggers the control box. The control box is a Berkley Nucleonics Model 565 pulse generator which connects the pre-detonator and hydrogen/oxygen microsolenoids to the PDE control system. The test section (Fig. 3.3) is attached to one of the cylinder heads of the PDE, shown in Fig. 3.2. The head of the PDE is shown at the left of Fig. 3.3. The fuel/air mixture flows out of the cylinder head and down the steel tube to the test section.
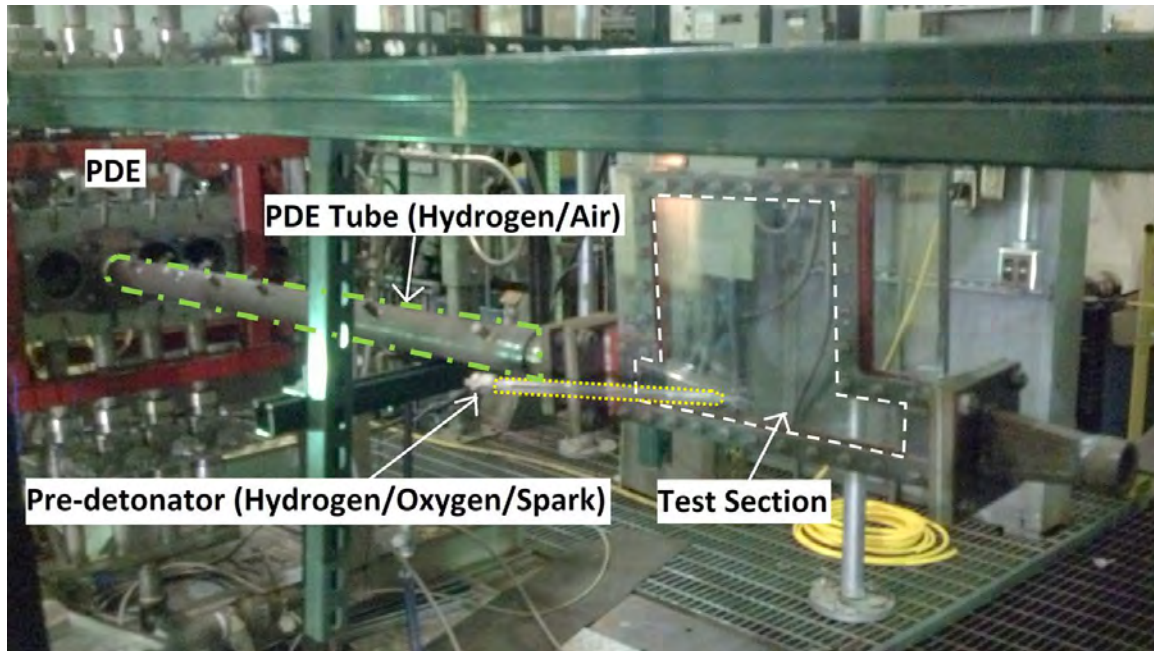
Figure 3.2. Test rig attached to PDE

3.2 Test Rig

In the first experiment the PDE regulates equivalence ratio and provides a structure on which to attach the test rig. The test rig consists of a steel center plate with two polycarbonate viewing windows sandwiched between two steel holding brackets. The steel center plate (seen in plan view of Fig. 3.3) setup leaves a 6.35 mm channel in between the two viewing windows. The polycarbonate windows are 12.7 mm thick. The upstream side (left side of Fig. 3.3) of the test rig connects to the PDE, while the other side opens to the room (right side of Fig. 3.3). The test section is 305 mm tall and 406 mm long.

The pre-detonator attaches to the window at various inclination angles (Fig. 3.4). One end connects to the window using JB Weld to secure the steel tube to the polycarbonate window. This thesis refers to the "right" direction as the direction of the pre-detonator, while the "left" direction is the opposite.
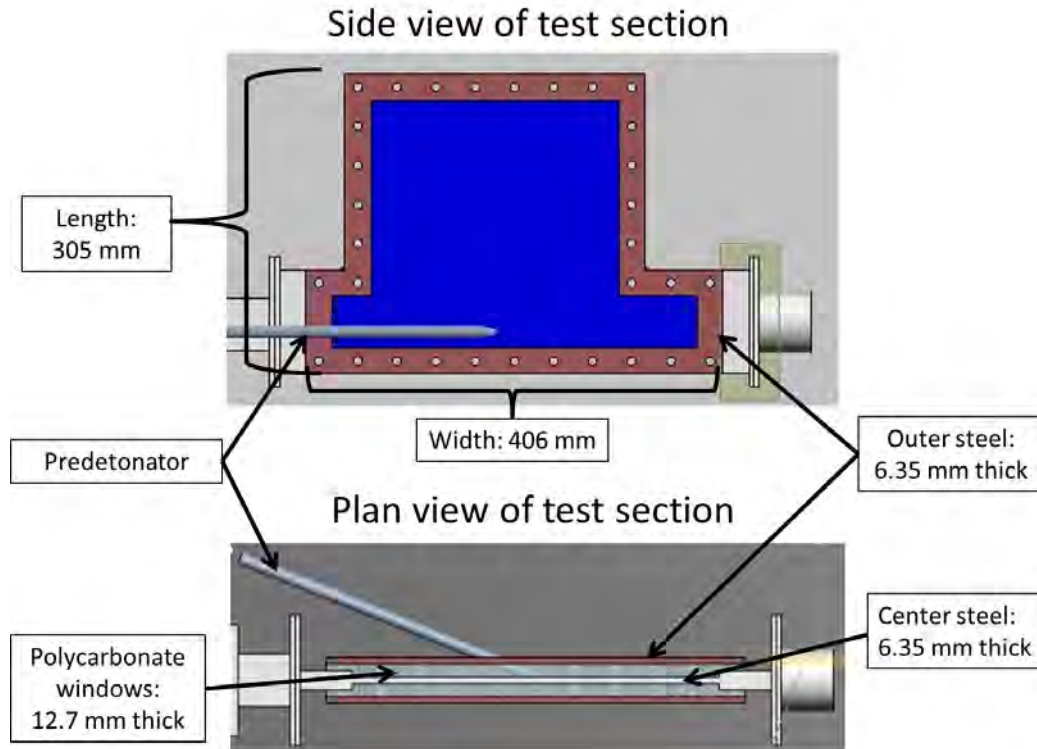
Figure 3.3. Side and plan view of test section
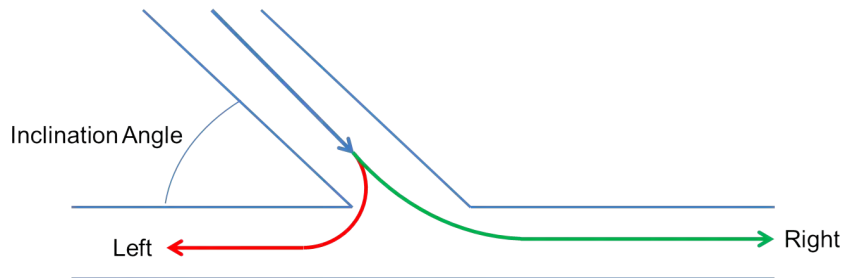

Figure 3.4. Visualization of the inclination angle

The inlet end of the pre-detonator connects to a supply of hydrogen (250 psi), oxygen (200 psi) and a spark plug. During normal operation the PDE uses the engine spark plugs and then allows the flow to transition to detonation as the wave travels down the tube. For experiments conducted in this thesis however, the spark comes from the end

of the pre-detonator. The sequence of events shown in Fig. 3.5 include filling the PDE
tube with air and hydrogen to a specified equivalence ratio. Next, the pre-detonator fills
with hydrogen and oxygen for 140 milliseconds in 7 millisecond bursts (bursts allow
cycling of the inlet valve to prevent electrical burnout). Finally, at the completion of the
fill the spark plug ignites to start detonation in the pre-detonator tube. Typically the first
two signals charge the ignition coil and the spark plug fires on the third signal.
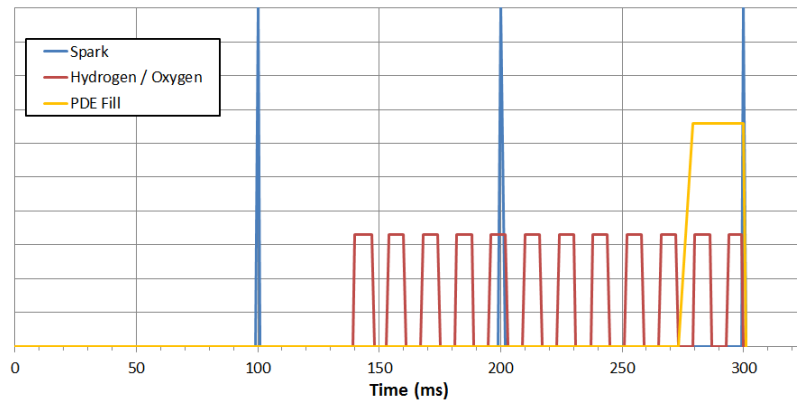

Figure 3.5. First test timing schedule. Note: Amplitudes are used for visualization only

For the first channel test run, pre-detonation tubes were stainless steel, 6.35 mm
Outer Diameter (OD), 3.175 mm Inner Diameter (ID), and of lengths 25.9 cm, 31.5 cm
and 52.8 cm, for the 45°, 22° and 11° cases, respectively. Each tube had a 13 mm thread
tapped to a depth of 13 mm at the upstream end to create a spiral for promoting DDT
within the pre-detonator tube.

The final test examined the effect of a step diameter change in a pre-detonator
attached to a narrow channel. In addition to testing the new pre-detonator scheme,
different wedge geometries were added in an attempt to add directionality to the shock
wave exiting the pre-detonator as shown in Fig. 3.7. Three different wedges, with angles
of 30°, 45° and 60° were placed into the channel at the location where the pre-detonator

enters as shown in Fig. 3.8. The wedges were 6.35 mm thick and made of mild steel.
Each wedge was secured to the bottom channel with string which looped through holes
(blue dashed line in Fig. 3.8) drilled into the wedge and around the bottom steel plate.
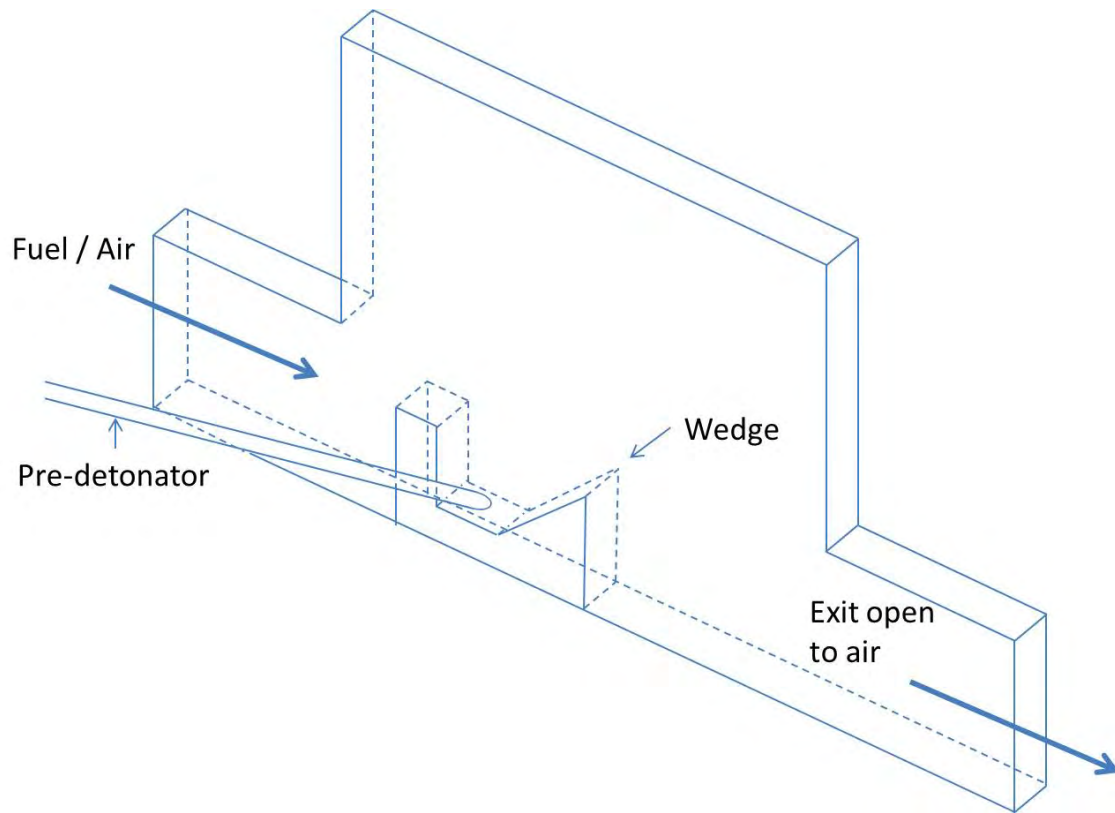
Figure 3.6. Wedge placed into the simulated channel
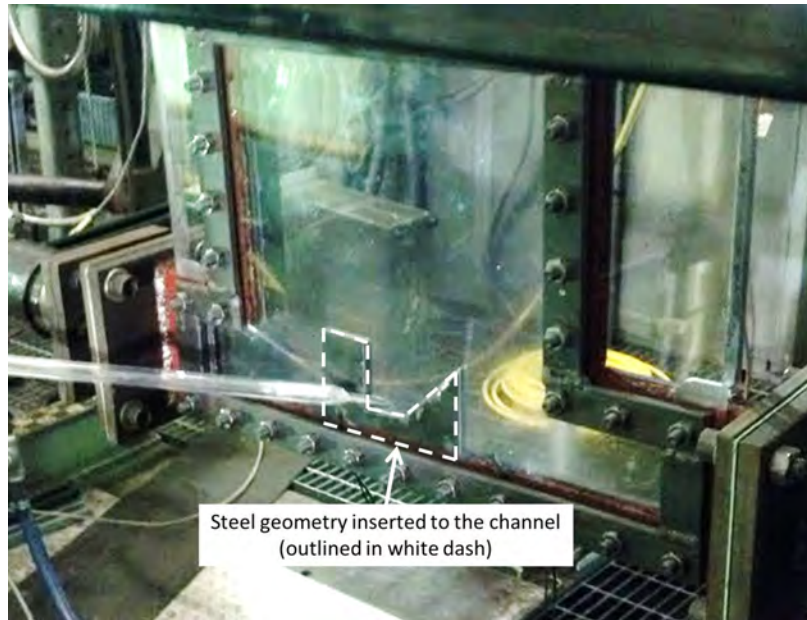
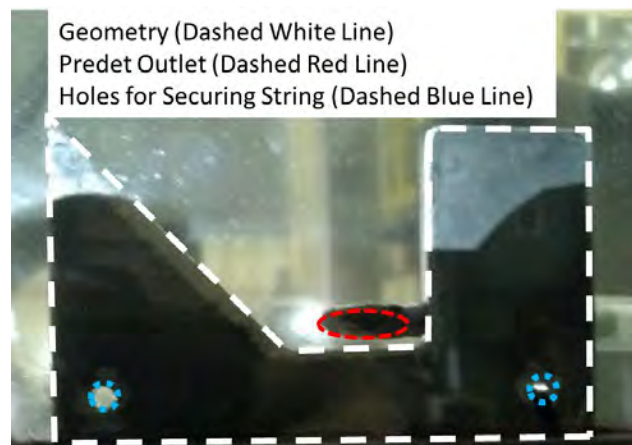Figure 3.7. Wedge geometry placed into the simulated RDE channel

Figure 3.8. Predetonator outlet lies directly above wedge geometry

The pre-detonator for the final set of testing is composed of different aspects taken from previous testing and is shown in Fig. 3.9. The pre-detonator had an OD of 13 mm and an ID of 6.35 mm, and was at an inclination angle of 22°. The inlet of the

pre-detonator had a 25 mm spiral that was threaded with a 8 x 1.25 mm tap. The inlet also had a step change in diameter at 25 mm, that reduced the diameter from 6.35 mm to 3.5 mm. A step change was also placed 25 mm from the exit, each step was approximately 6.35 mm long. The pre-detonator was made of polycarbonate tubing and the end was placed over the 6.35 mm stainless steel tubing, which was attached to the polycarbonate window from the previous tests.
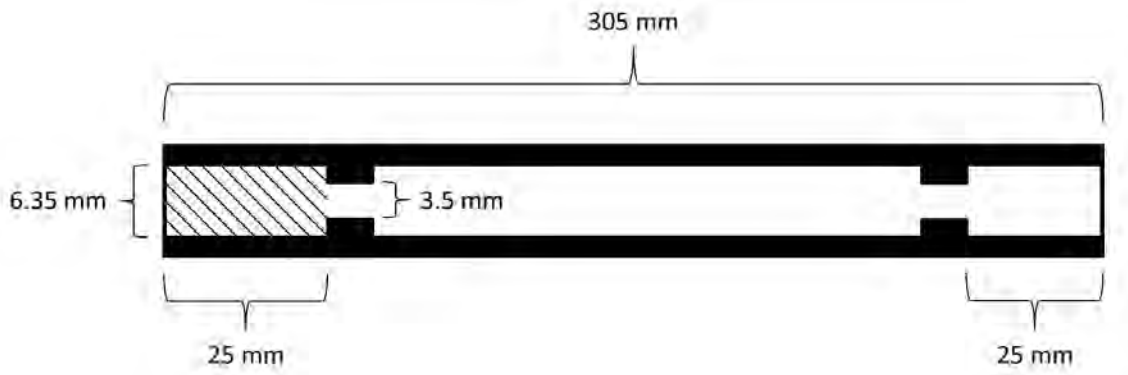

Figure 3.9. Sketch of pre-detonator used in final test

The ignition coil for the spark plug was upgraded for the final test, and ensured the spark fired on the first signal each time. Therefore the timing schedule for the final test included only one signal to the spark plug.

The wedge geometry (Fig. 3.10) placed into the channel had three primary benefits. The first benefit is the bottom base plate was raised to being right below the pre-detonator exit, ensuring that the shock does not separate and lose energy while traveling downward. The second benefit is the 90° wall on the left side, which acts as a barrier to the detonation traveling in the wrong direction. The third benefit is the wedge, which helps to keep the detonation wave attached.

43

Figure 3.10. Channel geometry with 30°, 45° and 60° wedges

3.3   Pre-detonator

The purpose of the pre-detonator testing was to confirm the presence of detonation in the first test and develop consistent detonation locations. The exit flows were also observed and velocities were measured and compared to where DDT occurred within the pre-detonator tube.

The pre-detonator testing consisted of a supply of hydrogen, oxygen and a spark plug at the inlet and open to air at the outlet. The pre-detonator is used to supply the initial detonation wave. Figure 3.11 shows the set-up of the pre-detonator test. The hydrogen and oxygen supply were matched to the RDE with pressures regulated to 250 psi and 200 psi, respectively.

Two pre-detonators were tested with an OD of 13 mm and 6.35 mm, and with an ID of 6.35 mm and 3.4 mm, respectively. The pre-detonator with a 6.35 mm OD was tested threaded to produce the effect of a Schelkin spiral discussed in Sec. 2.3.3.1 and shown in Fig. 3.12. The tap used to add the threading was 4 x 0.7 mm. The spiral was added to test its effect on the DDT location within the pre-detonator tube. The spiral lengths tested were 0 mm, 13 mm, 25 mm and 33 mm.

The pre-detonator tests were run on a timing schedule similar to the tests run with the pre-detonator attached to the channel. Each pulse for the hydrogen and oxygen micorsolenoids was 14 ms long to allow for 7 ms open and 7 ms closed cycling. The
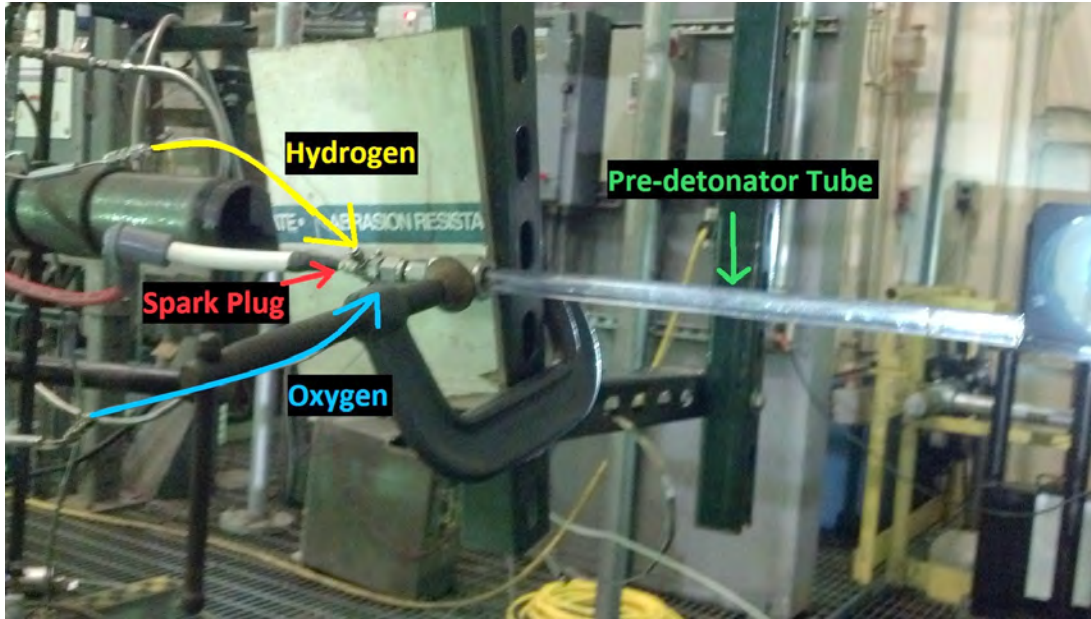
Figure 3.11. Pre-detonator testing set-up

Figure 3.12. An example of pre-detonator threading on 6.35 mm OD tube

hydrogen and oxygen pulsed 10 times, each with a width of 7 ms. The spark plug did not fire on the first or second signal, therefore the spark signal was pulsed 3 times with a width of 2 ms, and waited 10 pulses. Finally the camera used for Schlieren started recording on the tenth pulse, with a width of 2 ms. The timing schedule is summarized in Table 3.1.

The pre-detonator testing on the 12.7 mm OD tubes was different from the 6.35 mm. In the 13 mm tests, two configurations were tested, but with a step diameter change

45

Table 3.1. Timing schedule for pre-detonator testing

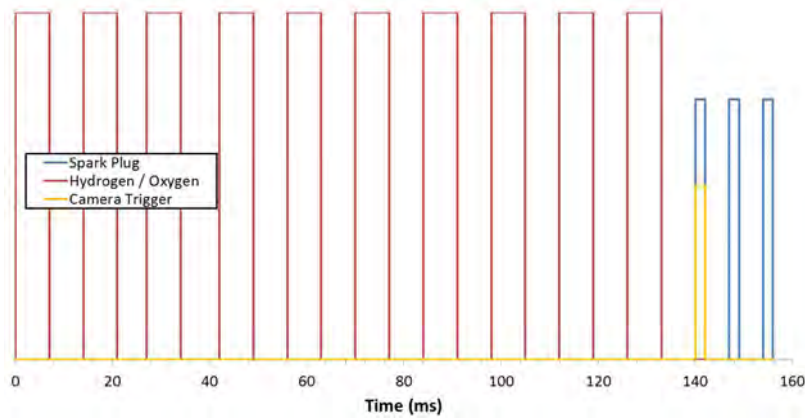| Device	Width (ms)	Number of pulses	Pulse wait
Spark Plug	2	3	10
Hydrogen and Oxygen	7	10	0
Camera	2	1	10

Figure 3.13. Pre-detonator timing schedule graph

to promote DDT instead of the carved Schelkin spiral. The two tubes are shown in Fig. 3.14. Figure 3.15 shows a closeup of a step change in diameter. Both tubes have a step diameter change at the beginning of the tube where the ID goes from 3.4 mm to 6.35 mm. The lower tube also has a step diameter change 25 mm from the outlet of the tube.

3.4 Camera Setup

3.4.1 Camera Specifications

The camera used during testing was a Vision Research Phantom v711. The camera has the ability to shoot at up to 680,000 frames per second (fps) at a reduced resolution of
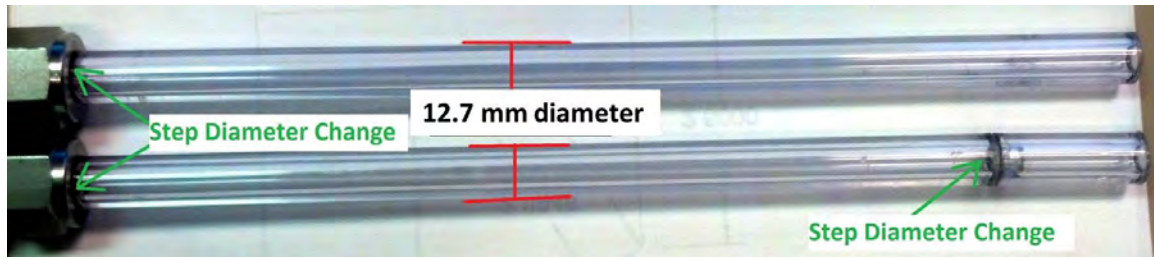
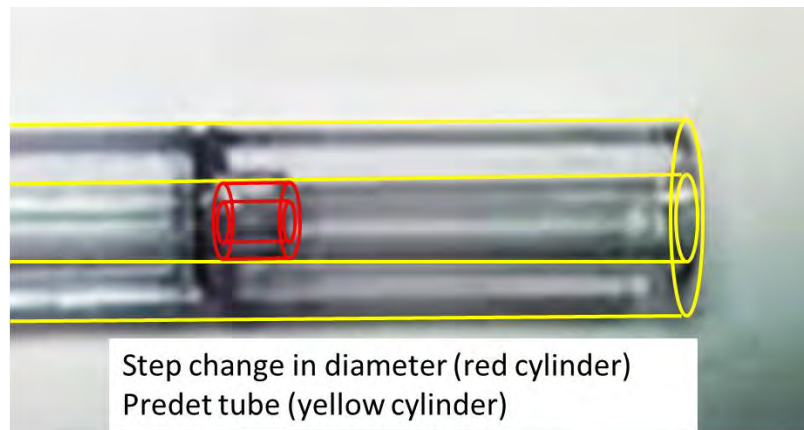Figure 3.14. Two configurations of 13 mm pre-detonator tested

Figure 3.15. Step change insert diagram

128 x 8 pixels. The testing conducted in this thesis was run at frame rates ranging

between 97,000 fps and 215,000 fps, with resolutions ranging between 512 x 128 pixels

and 128 x 128 pixels. The high frame rate allowed for video to be taken with a frame

every 10 μs. Videos were taken at the standard exposure time of 1 μs. In order to capture

each test a programmable auto-trigger was used as outlined in the timing schedule (Tab.

3.1), and video was taken for 3.5 seconds. The 3.5 second video length was more then

enough to capture each test, which typically occurred in 100 ms, but the unpredictability

of the spark necessitated the use of an extended time.

3.4.2   Diagram of Schlieren Setup

Schlieren imagery was used to see the various wave fronts. Schlieren photography is able to capture density changes in flow due to variations in the refraction of light. As outlined in Fig. 3.16, the Schlieren set-up consists of a light source, 2 focusing mirrors, 2 flat plate mirrors, a knife edge and a camera. The mirrors used had 305 mm diameters. The focal length for the focusing mirrors is approximately 2.5 m. Consequently the focusing mirrors are placed 2.5 m from both the light source and the camera. The knife edge is placed at the focal length from the second focusing mirror. When light is scattered by density changes within the flow field, the knife edge blocks the scattered light from reaching the camera and therefore a gradient is created within the flow.
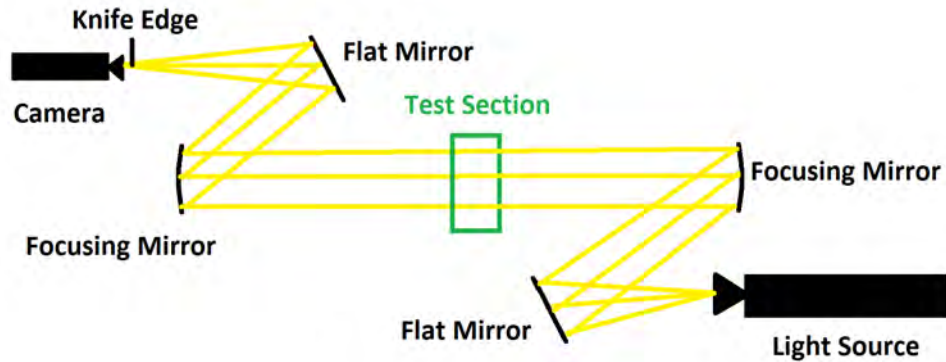
Figure 3.16. A diagram of the Schlieren imagery set-up

3.4.3 Example Schlieren Image

A still frame from one of the Schlieren videos is shown in Fig. 3.17 to provide a reference to the terms used. In Fig. 3.17, the pre-detonator is entering into the screen at a 45° inclination angle. The blackness at the bottom of the frame is the base steel plate and marks the bottom of the channel. Figure 3.17 shows the orientation of right and left, the shock wave and the combustion front.
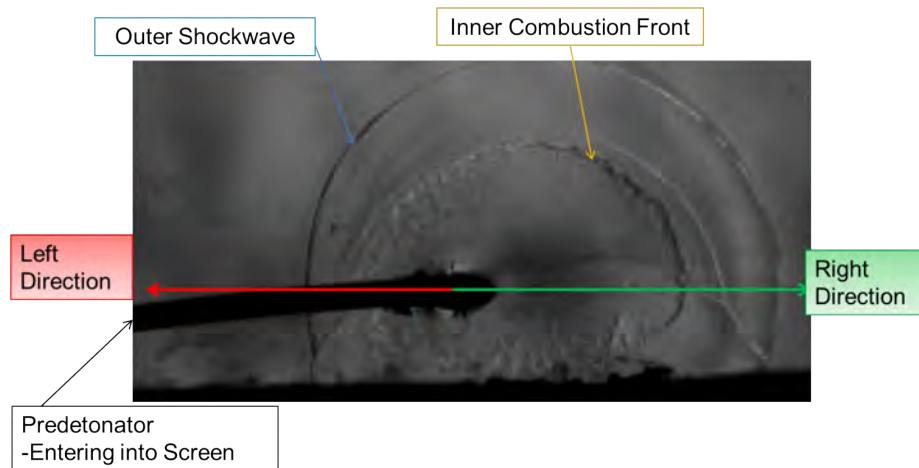

Figure 3.17. A Schlieren image with labeled parts

IV.   Results

4.1   Baseline Simulated Channel Test

4.1.1   Reorientation and Goals

The goal of the first test was to examine the transition of the detonation wave from the pre-detonator to the simulated RDE channel. This test was designed in order to test the effect of the angle of pre-detonator into the channel and the equivalence ratio in the channel. Equivalence ratios of 0.8, 1.0 and 1.2 were examined. In addition to the equivalence ratios, inclination angles of 11°, 22° and 45° were tested. Each test was run 3 times which led to a total of 27 tests. Videos were examined for exit flow velocities and separation distance between the shock and flame front.

4.1.2   Progression

The baseline experiment confirmed the theory of the deflagration to detonation transition occurring somewhere within the RDE itself and not directly transitioning at the pre-detonator exit (Fig. 4.1). The detonation wave cannot make the transition from the narrow tubing of the pre-detonator to the unconfined channel of the RDE without first decoupling.

When the frames from the video are shown in sequence (Fig. 4.1) there is evidence the decoupling occurs immediately once the tube end is reached. As seen in Fig. 4.1, the shock wave has decoupled from the combustion front by frames 4 and 5. The outer shock wave is the round smooth shape, while the inner combustion front has a more unsteady boundary. Due to the inability of the detonation wave to remain coupled out of the pre-detonator, the focus of further testing was on increasing the strength and directionality of the detonation wave, and ensuring that the wave which reflected off the bottom traveled in only the counter clockwise direction.

Figure 4.1. Video of 45° inclination into mixture with ϕ=1 (210,526 fps)

4.1.3 De-coupling of Detonation Front

Figure 4.2 shows the decoupling of the combustion front from the shock wave for the 45°, 22° and 11° angles, respectively. Each pre-detonator tube is 6.35 mm in diameter and is located 25 mm above the bottom steel plate. Figure 4.2 shows there is little variation of the decoupling location among the frames, but there is some variation in the shape of the exit flow. As the angle is decreased the surface area in which the tube is open to the channel is increased and skewed. The skewed opening leads to the 11° exit flow to be more oval in shape and the 45° exit to resemble a circle.
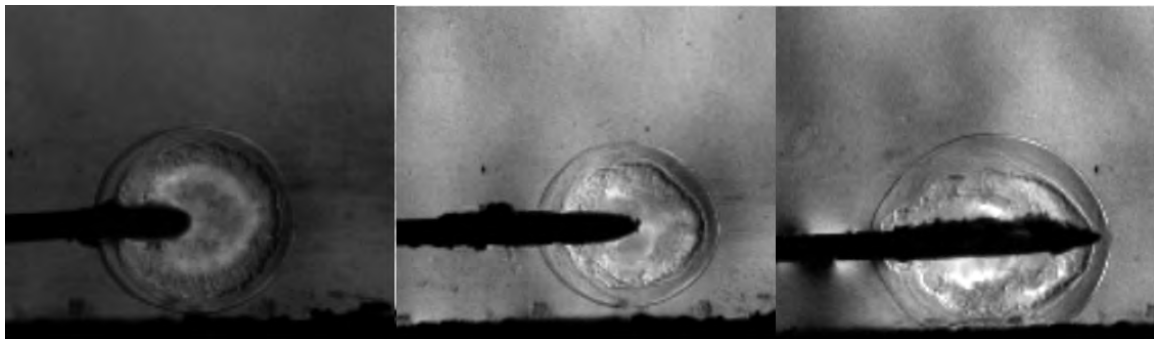

Figure 4.2. Fronts decouple prior to impact with bottom plate (45, 22, 11 deg angles)

4.1.4   Velocity of Combustion Front and Shock Wave

Figure 4.3 shows the average horizontal velocities for the combustion front and the shock wave taken for 100 ms after the waves were first seen in the high speed video. The "right" direction is the direction in which the pre-detonator is pointed. The "left" direction is the opposite. As expected, the velocities for the shock waves are higher than the combustion front. The velocities also show little difference among the varying angles. The results were expected to show an increase in velocity in the right direction for the lower angles. Instead, the velocities for the shock waves and combustion front remain close between the 11° and the 22°. The increase in velocities for the 45° are believed to be due to overfilling the pre-detonator tube with hydrogen and oxygen during the first tests.
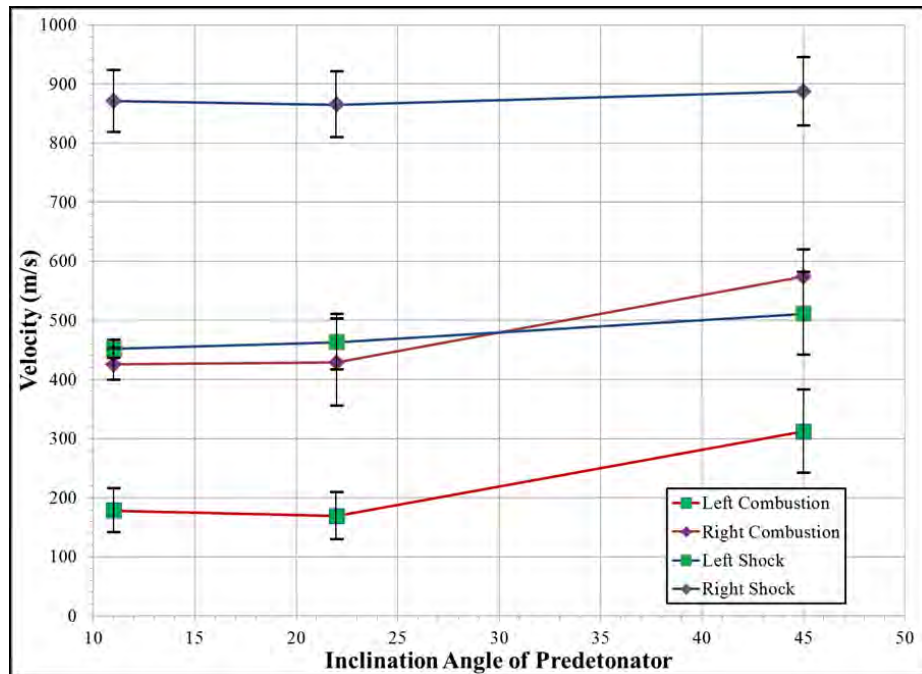

Figure 4.3. Horizontal velocities for combustion front and shock wave for 11°, 22° and 45° angles.

52

4.1.5   Mach Numbers

The Mach number for the shock waves was found in order to determine the effect of geometric wedges which were added later on. The Mach numbers were found for the rightmost point of the shock wave traveling in the horizontal direction. Equation 4.1 shows the combustion equation for $\phi = 1$.

$$2H_2 + (O_2 + 3.76N_2) \rightarrow 2H_2O + 3.76N_2 \tag{4.1}$$
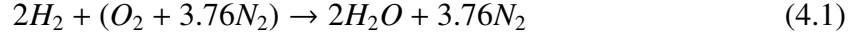
The specific gas constant was found through:

$$\frac{2\ mols\ H_2}{6.76\ mols} * \frac{2\ g}{mol} + \frac{1\ mols\ O_2}{6.76\ mols} * \frac{32\ g}{mol} + \frac{3.76\ mols\ N_2}{6.76\ mols} * \frac{28\ g}{mol} \approx 20.9\frac{kmol}{kg} \tag{4.2}$$

$$R_{specific} = 8,314\frac{J}{K*kmol} \ / \ 20.9\frac{kmol}{kg} \approx 397\frac{J}{kg*K} \tag{4.3}$$

The temperature, ratio of specific heats and specific gas constant were needed to find the speed of sound in air. The temperature in the test cell was 293 Kelvin. The ratio of specific heats was assumed to be 1.4 due to air being a diatomic gas at approximately room temperature.

$$a = \sqrt{\gamma RT} = \sqrt{1.4 * 397 \frac{J}{kg*K} * 293\ K} \approx 404\frac{m}{s} \tag{4.4}$$

The equation used to find the Mach number is:

$$M = \frac{V}{a} \tag{4.5}$$

Figure 4.4 shows how the Mach numbers for each of the three equivalence ratios tested. Figure 4.5 shows the Mach numbers for each of the inclination angles tested. The

"First to Second Frame" is the Mach number from the first frame of the video in which the wave was visible, to the next frame. For each test there was 8.9 μs between frames. Figure 4.4 shows the little variation amongst the three equivalence ratios. All of the Mach numbers are situated between Mach = 2.5 and Mach = 3. Similar Mach number results are seen when the Mach number is plotted against the inclination angle of the pre-detonator (Fig. 4.5). From the two Mach number plots there is evidence the detonation front will need to be "overdriven" in order to raise the velocity to Mach = 3.5 before exiting the pre-detonator tube, as discussed in Sec. 2.7.
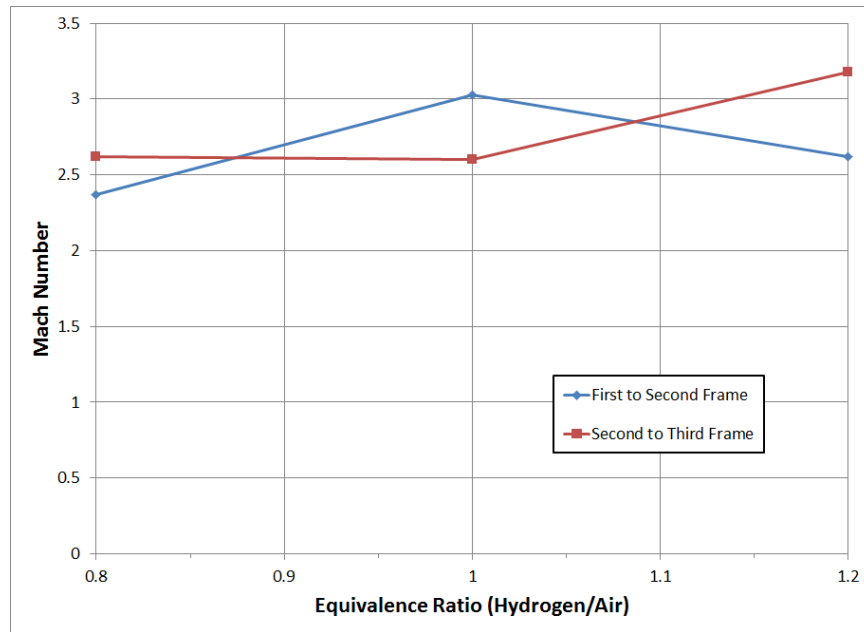
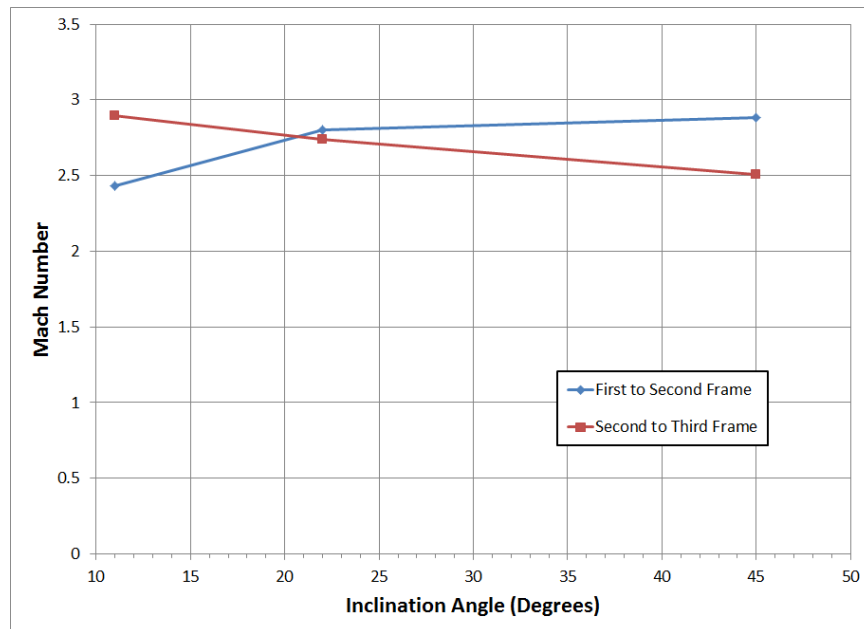Figure 4.4. Mach numbers of shock wave for $\phi = 0.8$, 1.0 and 1.2

Figure 4.5. Mach numbers of shock wave for 11°, 22° and 45° angles.

4.1.6   Exit Shape and Shock Reflection

The frames in Fig. 4.6 show the side view as the detonation wave leaves the pre-detonator and enters the narrow channel. The following descriptions focus on the circles near the left corner. The first frame depicts a frame after the wave front reflects off the bottom plate and interacts with the combustion front, as indicated by the dark 45° line within the red circle. The second frame captures reinitiation of the detonation front as the reflection joins with and pulls the combustion front forward until the third frame where the detonation front decouples. This behavior of reinitiation was seen in both the left and right direction, but only the left direction is visible in Fig. 4.6. The reflected shock traveling in both directions indicates that there is not a strong directionality imparted on the detonation wave entering the channel. The shock wave traveling in either direction could re-initiate a detonation front and result in the bifurcation mode discussed earlier. Further testing sought to eliminate the detonation traveling to the left and strengthen the detonation in the right.
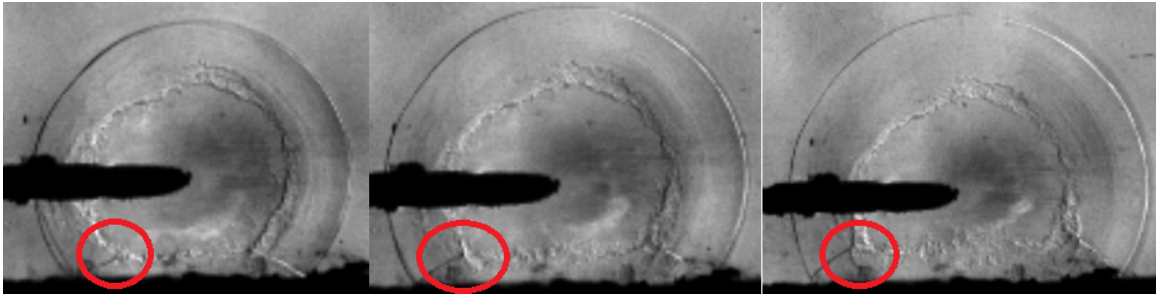

Figure 4.6. Still frame shots of 22° inclination into ϕ=1 (119,089 fps)

4.1.7 Interaction Between Reflected Shock and Combustion Front

Figure 4.7 shows the interaction between the shock wave reflecting off the bottom plate and the combustion front traveling in the left direction. In the 45° image, the interaction occurs when the shock wave and the combustion front are still relatively close together, and there is a resulting bright flash. The bright flash indicates a density change brought on by re-ignition of reactants as the shock wave travels down the channel. In the 22° image, the interaction occurs slightly farther back of the leftwards traveling shock wave, and the flash is approximately half the length of the 45° pre-detonator. Finally, the 11° pre-detonator produces an interaction point far behind the left traveling shock wave, and as such no flash occurs. Figure 4.7 implies that as the angle of the pre-detonator is decreased, the pre-detonator must be lowered to get the reflected shock to interact earlier with the combustion front, in a similar manner as the higher angle. By lowering the pre-detonator for the lower angles, the reflected shock will not take as long to reflect off the bottom plate and interact with the combustion front, and will therefore occur closer to the decoupling location.
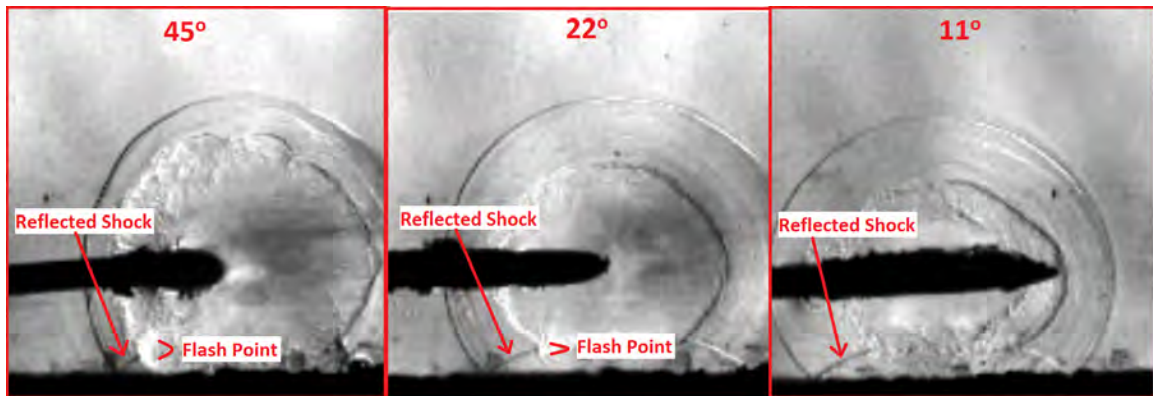

Figure 4.7. Still frame shots of 45°, 22° and 11° re-initiation point

4.2　6.35 mm Pre-detonator Testing with Different Spiral Lengths

4.2.1　Reorientation and Goals

The goal of the first pre-detonator test was to discover if detonation was occurring within the pre-detonator and to test the effect of a spiral carved into the inside of the tubing. Spirals of lengths 0 mm, 13 mm, 25 mm and 33 mm were tested. In addition to the spiral, the 33 mm test also had a step change in diameter created before tests were run. The other spirals did not have the step. The videos were analyzed to determine which spiral produced the most consistent DDT location. Videos were examined for exit flow velocities and separation distance between the shock and flame front. A bright flash was present in the videos when DDT occurred in the pre-detonator tubing. The location of DDT was then determined from the flash.

4.2.2　Exit Flow

Figure 4.8 shows the exit region for polycarbonate tubes of 305 mm length visualized with the high speed camera. The left frame is for a tube internally threaded to a depth of 33 mm at the inlet side, while the right frame is a tube un-threaded. The picture on the left shows a nearly spherical exit plume for the DDT case occurring more than 280 mm upstream (see run 1, Table 4.1 for details). The right picture shows a narrowed, jet-like plume for run 4 with DDT occurring within 50 mm of the tube exit. It is hypothesized the jet-like plume will provide a beneficial directionality which could be useful in creating a detonation in the RDE that is more likely to proceed in the direction of the plume rather than randomly turning in an opposite direction as previous testing has shown to occur.

In the pre-detonator test setup a tap was used to create different thread lengths to see the effect on DDT location. Table 4.1 shows the relationship between the thread length and the location along the tube in which the DDT flash was observed. The 33 mm threading was the maximum length the tap could thread the tubing, and also produced the
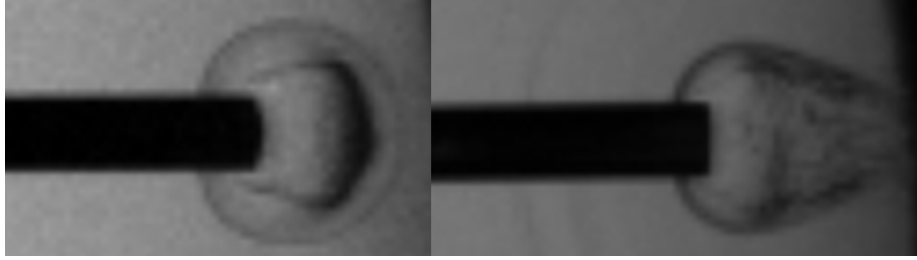
58

Figure 4.8. Left is where DDT occurred early in the tube. Right is a test where DDT occurred at the end of the tube.

best results (earlier DDT). The results proved what was expected in that some sort of internal tripping device is necessary to help facilitate the DDT. On average the tubing used during the first test had a length of 305 mm and threading of approximately 13 mm, and therefore detonation can be confirmed in the initial testing.

    Prior to running the 33 mm cases the polycarbonate melted due to the heated Swagelok fitting, resulting in a nozzle type shape located at approximately 5 mm (See Fig. 4.9). Interestingly, the resulting step area change caused the DDT to occur earlier than expected (expectation was for about 100 mm from the tube inlet). Furthermore the DDT locations were fairly consistent unlike the other spiral length cases. From the tabularized data in Tab. 4.1 it can be reasoned that while threading is necessary to produce DDT, a step change in diameter has a far greater impact on consistency. The 33 mm threading cases had the nozzles for all tests, but the other cases did not.

Figure 4.9. Melted 33 mm threaded tubing formed a nozzle shape

59

Table 4.1. Location of DDT in the pre-detonator tube

Run	Thread Length (mm)	Location from Tube Inlet (mm)
1	33	15.9
2	33	15.5
3	33	7.1
4	0	257.5
5	0	No DDT
6	0	183.4
7	0	189.8
8	0	No DDT
9	13	2.5
10	13	168.6
11	13	140.4
12	13	194.7
13	25	131.2
14	25	133.3
15	25	Cannot Determine
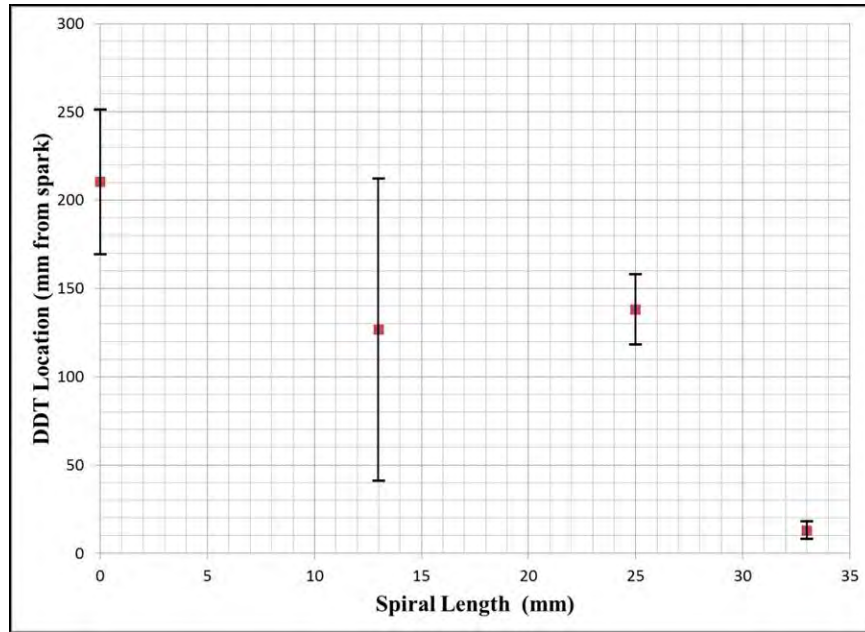
Figure 4.10. Averaged locations of DDT

Velocities were determined from evaluating successive video frames tracking the detonation wave front and are shown as the red line in Fig. 4.11. The velocities were calculated as the average velocity seen from the time of DDT to the time at which the wave front exited the tubing. Velocities did show a relation to the thread length. Higher velocity is believed to be a result of a much earlier, and consistent, DDT location with the longer thread lengths. Data is not shown for the 0 mm thread length because of inconsistent DDT locations, and several deflagration events did not transition. Figure 4.11 also shows the average velocity of the combustion front and the shock wave after exiting the pre-detonator tube. Figure 4.11 shows how the exit velocities appear to show a correlation with the spiral length from 0 mm to 25 mm, but not with the 33 mm spiral length.

Finally, it is worth examining the exit velocities from the tubing as compared to where DDT occurred. Figure 4.12 shows that as DDT is given less time in the tube to
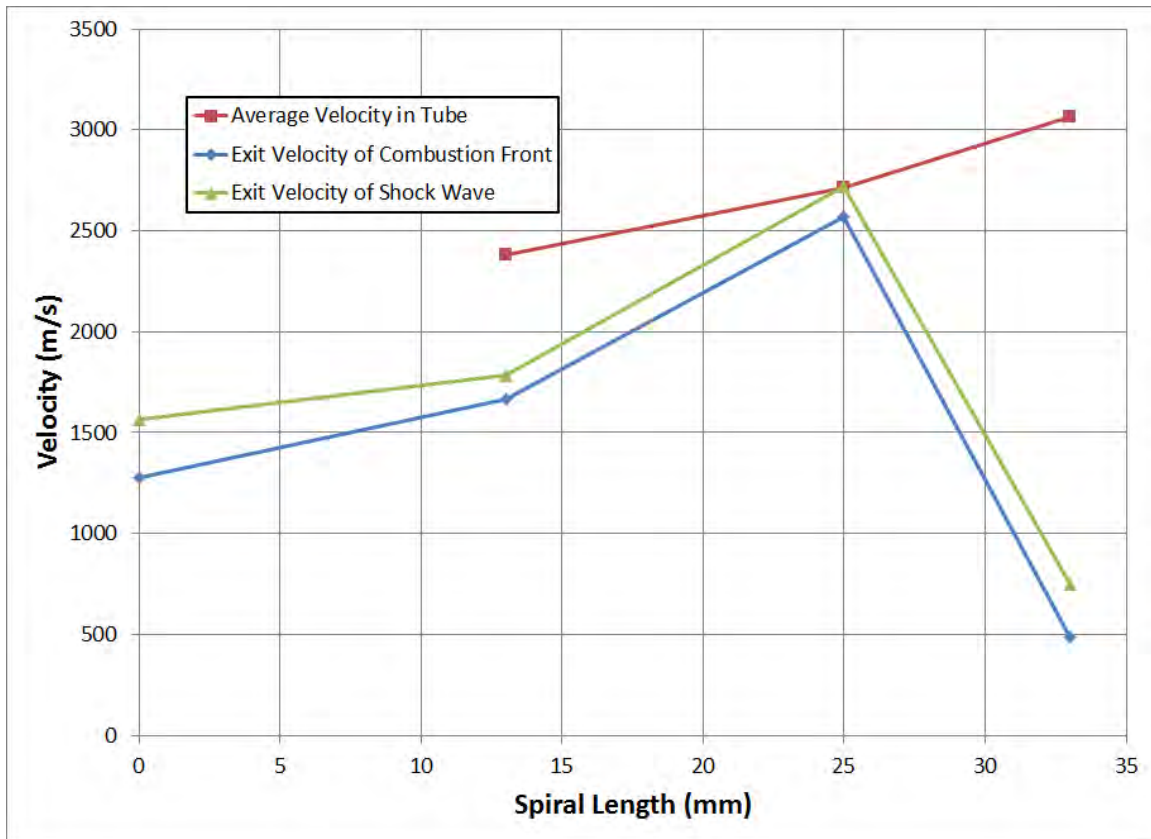
Figure 4.11. A plot of the detonation wave velocity for various Schelkin spiral lengths

reach steady conditions, the exit flow is not only far more concentrated in a jet, but also exits at a much higher rate. Further testing examined combining both a step diameter change and the late DDT results to get a focused jet traveling in one direction.

4.3 13 mm Diameter Pre-detonator Testing with Step Change in Diameter

4.3.1 Reorientation and Goals

The goal of the second pre-detonator test was to confirm the effect of the step change in diameter seen in the previous test. A step change in diameter was placed immediately at the entrance of the pre-detonator tube for both configurations. A step was also added to the exit of one of the pre-detonator tubes. This test sought to examine two
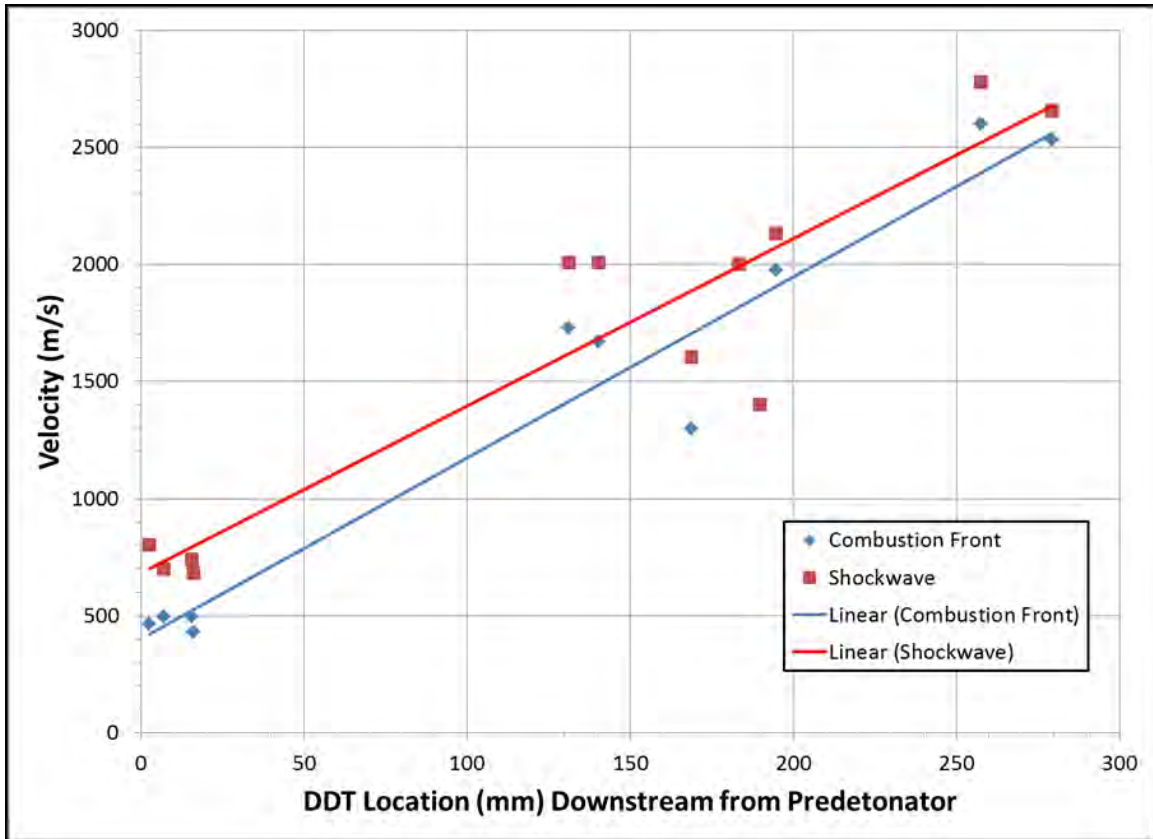
Figure 4.12. A plot of the detonation wave velocity for various DDT locations within tube

effects in the previous test which showed consistent DDT location with a step and higher

exit velocities for a later DDT location. The step change that produced consistent results

was placed close to the exit to determine if it would increase the exit flow velocity.

Videos were examined for exit flow velocities and separation distance between the shock

and flame front.

4.3.2   Exit Flow Analysis

The second set of pre-detonator tests were run in an effort to confirm the theory that

a step change in the inner diameter would overdrive the detonation and produce higher

exit velocities. For the 13 mm pre-detonator test, the same timing schedule from 6.35 mm

tests was used (as outlined in Table 3.1). The pre-detonator in the second set of tests had

an OD of 13 mm, with an ID of 6.35 mm and a step change in diameter reduced the diameter to 3.5 mm and was approximately 6.35 mm long. The exit velocities for the shock wave were taken for the first 4 frames ($\approx 40\ \mu$s) after the waves exited from the tube. The results in Fig. 4.13 show how a step change in diameter was able to overdrive the wave right before the detonation exited the tube. Overdriving the wave before exit led to roughly double the exit wave velocity.
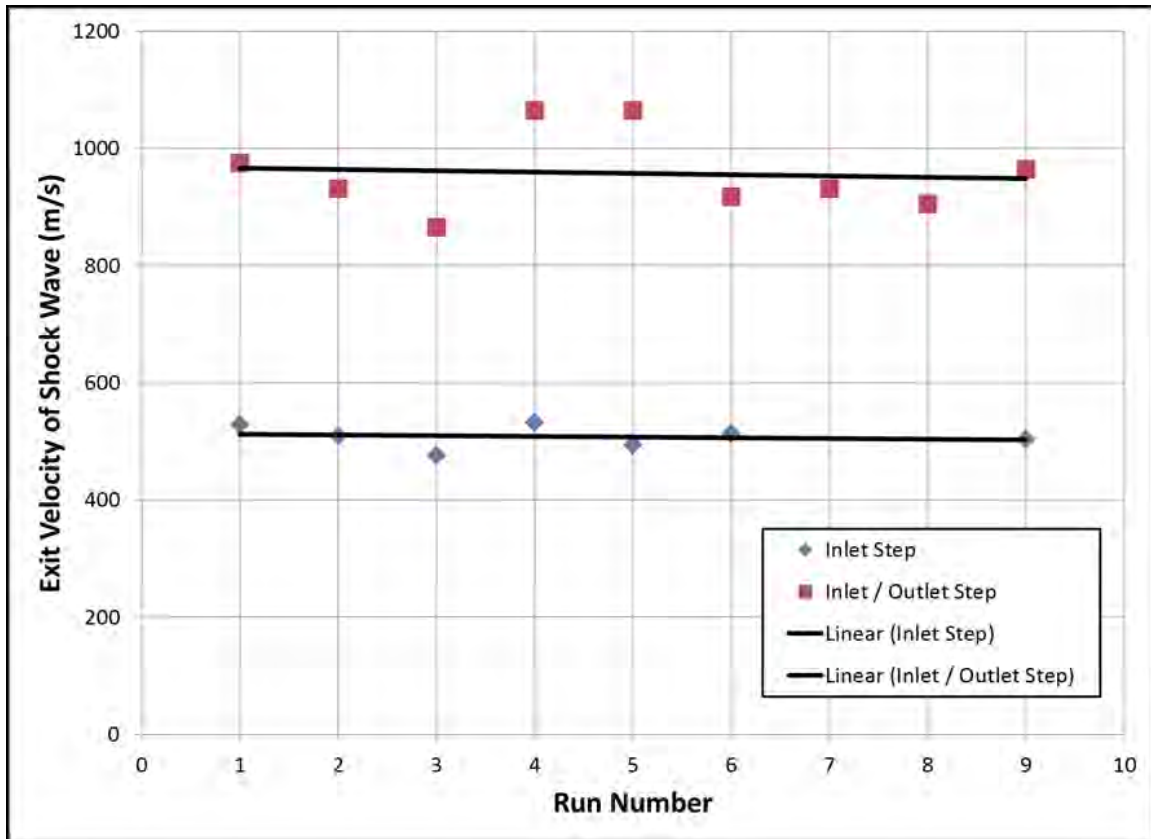

Figure 4.13. A plot of the exit velocity for the two 13 mm OD pre-detonator configurations

When the velocities are converted to Mach numbers (Fig. 4.14), the results for the overdriven wave are in the vicinity of Mach 3. Figure 4.14 shows the results for the 13 mm pre-detonator exiting into air in an unconfined space. The expectation is that when

the wave is confined and exiting into a reactive mixture of hydrogen and air, the Mach numbers will be higher. If the Mach is able to reach 3.5, then the decoupled detonation would be expected to show the same behavior to wedges placed in the flow, as outlined in Section 2.7. If a step is not added to the flow, as depicted by the blue markers in Fig. 4.14, then it is expected the geometry additions will not re-initiate the flow. The pattern of higher velocities evidenced by plotting the results of the previous tests, necessitated including a step area change before the exit of the pre-detonator.
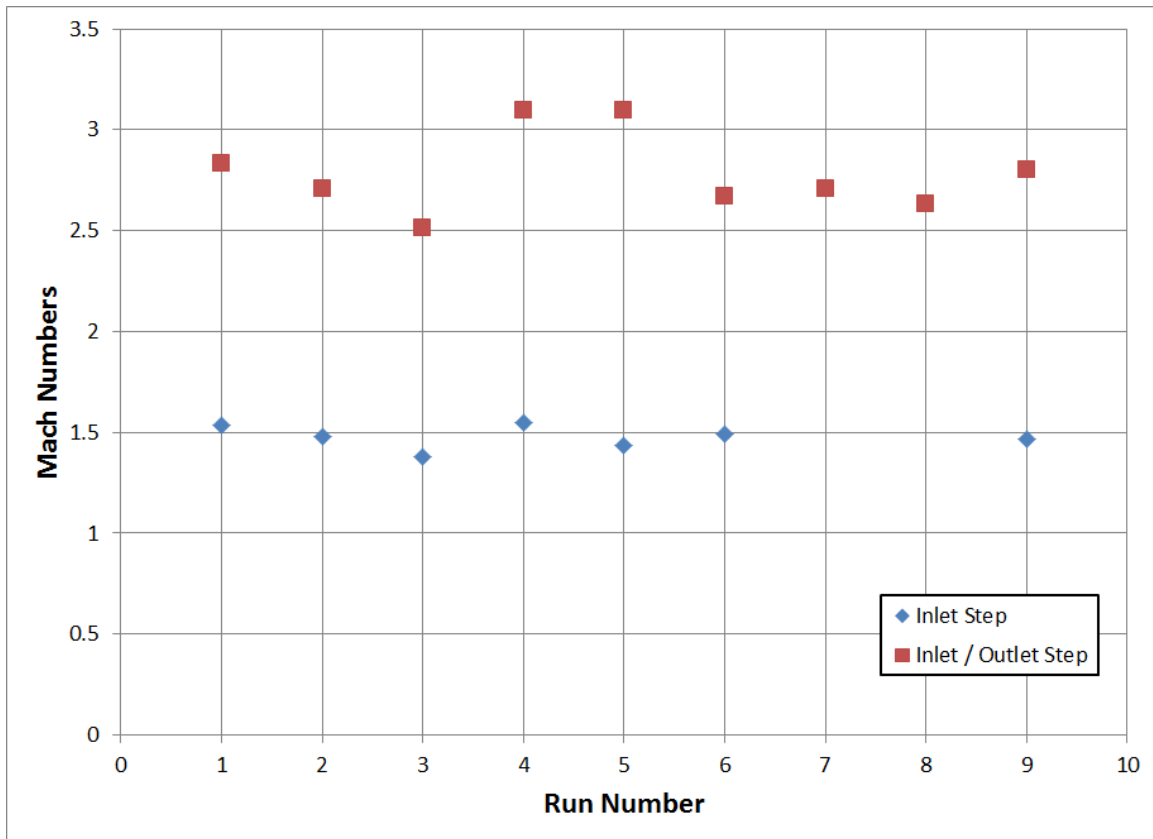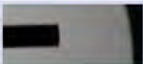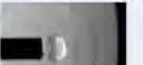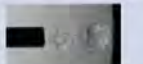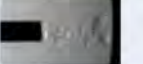
Figure 4.14. A plot of the exit Mach numbers for the two 13 mm OD pre-detonator configurations

Adding a step change in diameter at the exit produced noteworthy exit flows. Figure 4.15 shows the exit flows for Run 1-1 (inlet step only) and Run 2-1 (inlet and outlet steps). In the first frame for each run, a circular wave exits the tube at a velocity typically around 500 m/s. The first wave to exit most closely represents the sub-critical case, and as such the detonation wave decouples from the combustion front immediately upon exiting the tube. In Run 1-1, the following set of frames show a reaction zone exiting the pre-detonator. The combustion front follows the shock-wave out of the pre-detonator tube, in a spherical shape. Video analysis shows how the reaction zone appears to dissipate after the second frame, but later on the flow reignites and produces a jet which holds at the exit.

Run 2-1, shown on the right side of Fig. 4.15, produces similar results to Run 1-1 at the beginning. The same circular, smooth shock-wave exits the tube, and then the reaction front seems to dissipate shortly thereafter. However the difference is in the secondary exit flow from the tube, where Run 2-1 produces a clear detonation wave. Instead of jetting like Run 1-1, a coupled detonation front exits the tube at around 1200 m/s in Run 2-1 . In Run 2-1 the detonation front does not re-couple after the initial de-coupling. The initial exit flow, seen in Frame 1, shows an exit flow more analogous to the sub-critical diameter case discussed in the Literature Review chapter. Due to the critical diameter similarities, if Run 2-1 flow was entering the RDE channel, the hypothesis is that a step change in diameter at the outlet would have a much greater chance of re-initiating than in Run 1-1.

Time from Trigger	Run 1-1
16780μs	
16835μs	
16892μs	
16950μs	
17010μs	
17065μs	
17122μs	
17180μs	
17236μs	
17294μs	
17351μs	

Time from Trigger	Run 2-1
16780μs	
16835μs	
16892μs	
16950μs	
17010μs	
17065μs	
17122μs	
17180μs	
17236μs	
17294μs	
17351μs	

(a) Run without step change at exit   (b) Run with step change at exit

Figure 4.15. Exit flow for the two 13 mm OD pre-detonator configurations

4.4 Simulated Channel with Redesigned Pre-detonator and Wedges

4.4.1 Reorientation and Goals

The goal of the final test was to examine the effect of the pre-detonator step diameter change before entering the simulated channel and to implement wedges into the flow. Tests were conducted with no wedge in order to single out the step change in diameter as a variable and determine if the step helped to directionalize the flow. Additionally, wedges of 30°, 45° and 60° were tested in the simulated channel. The goal of the wedges was to force the detonation to travel in only one direction. Videos were examined for exit flow velocities and separation distance between the shock and flame front. The plots for this section have the separation distance between the shock wave and the flame front (in mm) on the left and the shock wave velocity (in m/s) on the right.

4.4.2 Contour Plot Creation

The following contour plots in this section were created with a code developed by Stevens[26]. The camera outputs files in the ".cine" file format. The ".cine" files are loaded into MatLab and converted to matrices of pixel values to be interpreted and displayed (Fig. 4.17). After loading the files into MatLab, the difference is taken between the frame of interest and the first frame of the set (Fig. 4.18). By measuring this difference, any marks on the windows left by previous shots are removed from the picture and only the flame and shock remain. Next, the shock wave and flame front get marked separately by the user and are converted to an array which is added to a structure file (Fig. 4.19). After marking the frames of interest, a separate program creates arrays of separation distance and shock wave velocity with the user inputting mm/pixel and time steps between frames. To create the distance and velocity arrays the program interprets the shock wave and finds the next point by approximating a line normal to the shock wave curve.
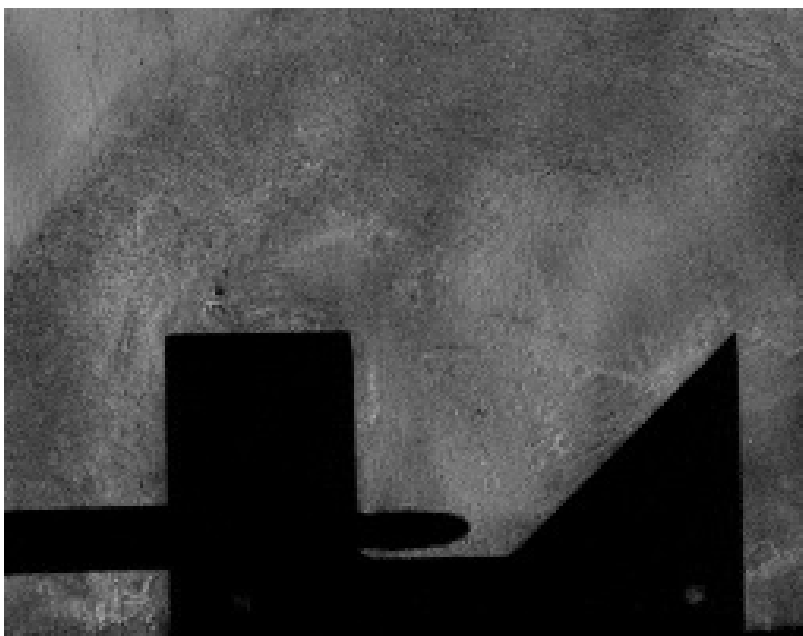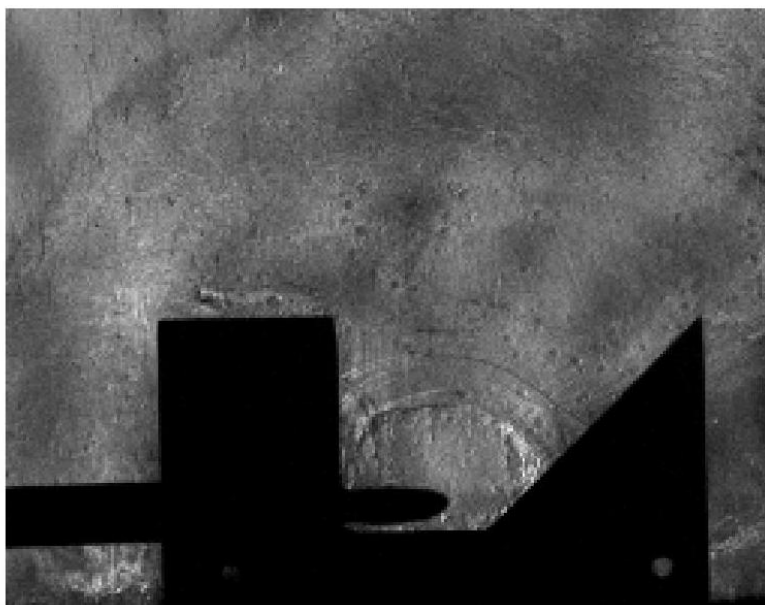
Figure 4.16. First ".cine" frame grab

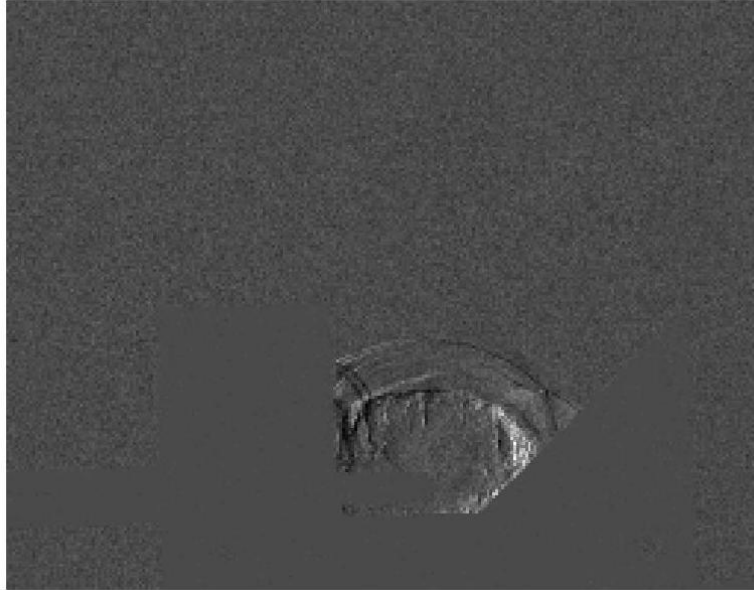Figure 4.17. Raw ".cine" frame grab

Figure 4.18. Difference between 1st and current frame
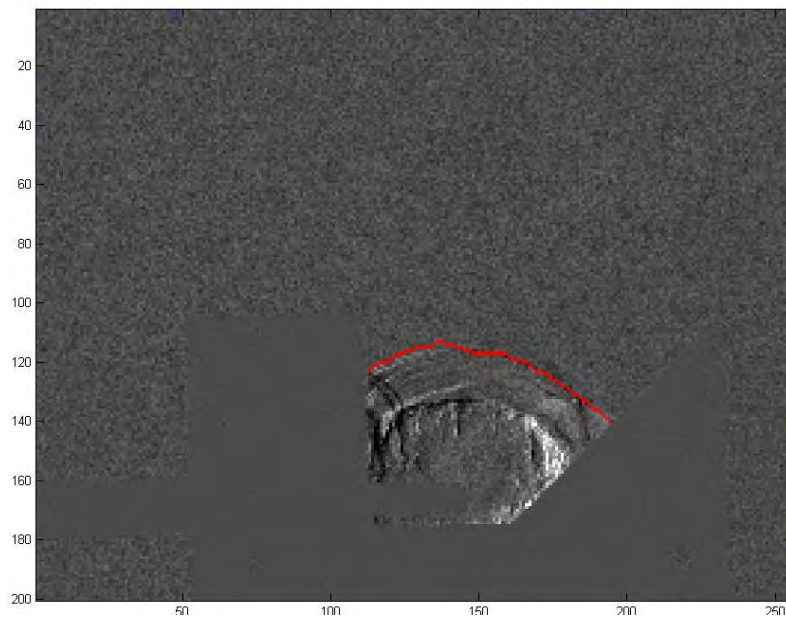
Figure 4.19. Marking the shock wave

4.4.3   Pre-detonator step effect into simulated channel

The final test allowed for all of the previous results to be combined to see if overdriving the detonation wave and adding geometry would allow for an improved transition from pre-detonator to the channel. Figure 4.20 shows the original test on the left (no step in pre-detonator) and the second test on the right (step 25 mm from the pre-detonator exit). When the final test runs are compared to the baseline tests runs (Fig. 4.20), one can see how the circular expansion of the flow leaving the pre-detonator has been replaced by a jet. After seeing late DDT in the pre-detonator tests it was hypothesized that the jet would increase the distance in which the wave remains coupled in the right direction. Figure 4.20 confirms this theory as the detonation wave remains coupled for $\approx$ 30 mm without a step (left in Fig. 4.20) and for 50 mm with a step 25 mm from the pre-detonator exit(right in Fig. 4.20). Runs 2 through 4 (Fig. 4.21) have a step change in diameter approximately 40 mm from the exit. Figure 4.21 shows the directionality of the wave by the lower separation distances in the right traveling direction. The detonation wave decouples in the right direction at approximately 40 mm for Runs with the step, and at only 10 mm in the left direction, as measured from the pre-detonator outlet.
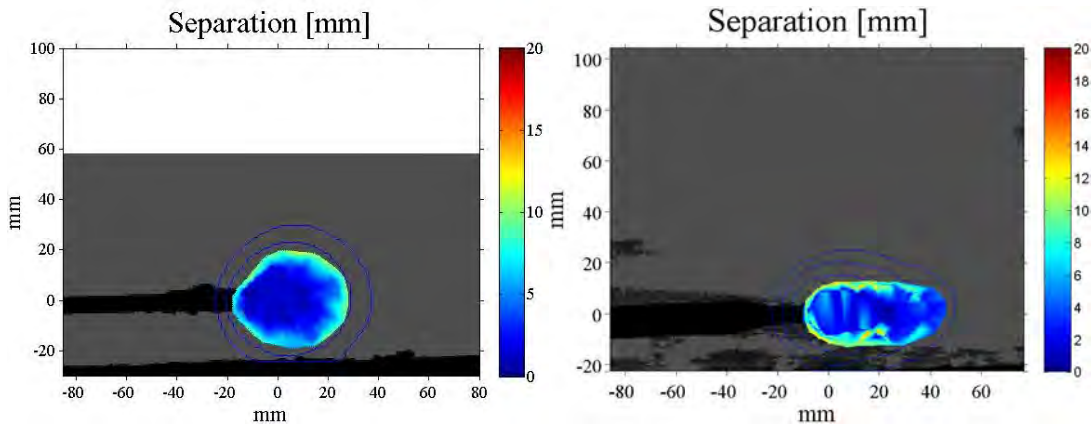
Figure 4.20. Separation distance without step at exit (left) and with step at exit(right)
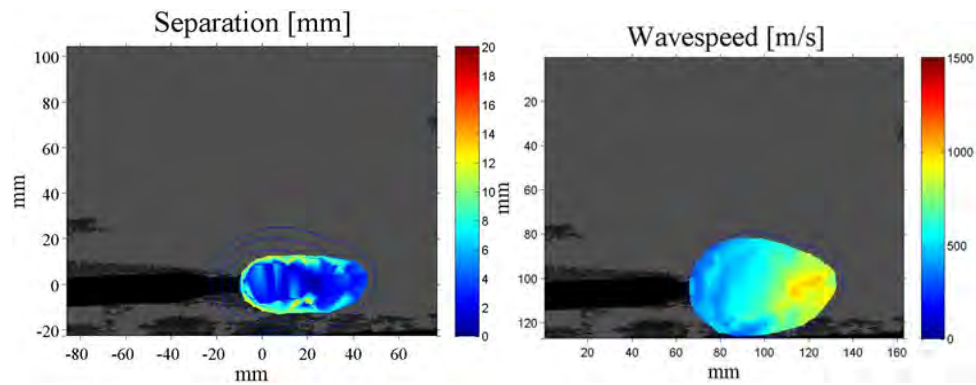
(a) Run 2: Separation distance (mm)

(b) Run 2: Shock wave velocity (m/s)
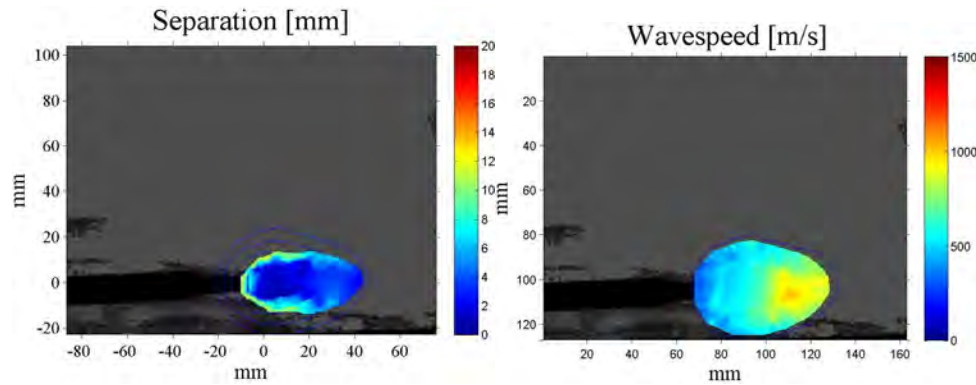
(c) Run 3: Separation distance (mm)

(d) Run 3: Shock wave velocity (m/s)
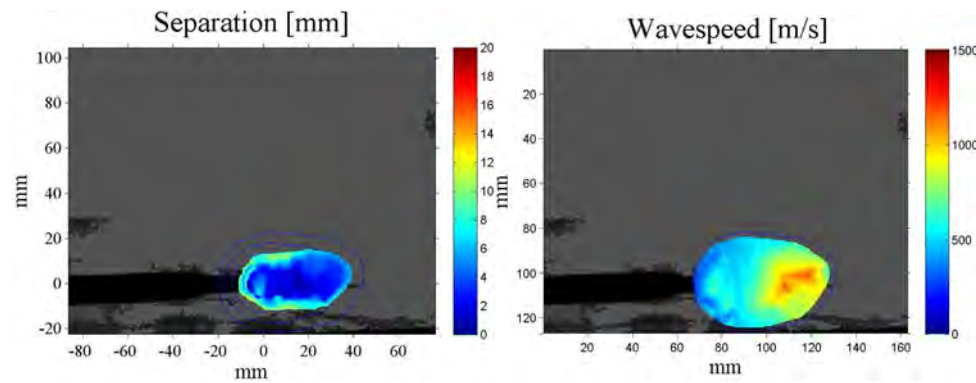
(e) Run 4: Separation distance (mm)

(f) Run 4: Shock wave velocity (m/s)

Figure 4.21. Separation distance and shock wave velocities for no geometry with step at exit

4.4.4 30° Wedge

The first geometry added into the channel was a 30° wedge. For two of the runs (Runs 6 and 7, Fig. 4.22) the detonation wave remain coupled after exiting the pre-detonator and traveling up the wedge. For Run 6 the wave decoupled at approximately 42 mm from the pre-detonator exit, and for Run 7 the decoupling occurred 45 mm from the exit. Frames (b) and (d) show the speed of the shock wave from frame to frame. The wave speed graphs shows that a focused jet was created by a step change, as evidenced by how the velocity is primarily focused in the right direction. Also of note here is that by approximating a speed of sound for hydrogen and air to be 400 m/s, the wave exit velocity is above the Mach = 3.5 that was desired.

(a) Run 6: Separation distance (mm) (b) Run 6: Shock wave velocity (m/s)

(c) Run 7: Separation distance (mm) (d) Run 7: Shock wave velocity (m/s)

Figure 4.22. Separation distance and shock wave velocities for the 30° wedge

Runs 5, 8 and 9 (Fig. 4.23) show the same 30° wedge in the channel. Frames (a), (c) and (e) show the separation distance between the shock wave and flame front. From analyzing the data presented in the aforementioned frames, the detonation wave decoupled immediately upon exiting the pr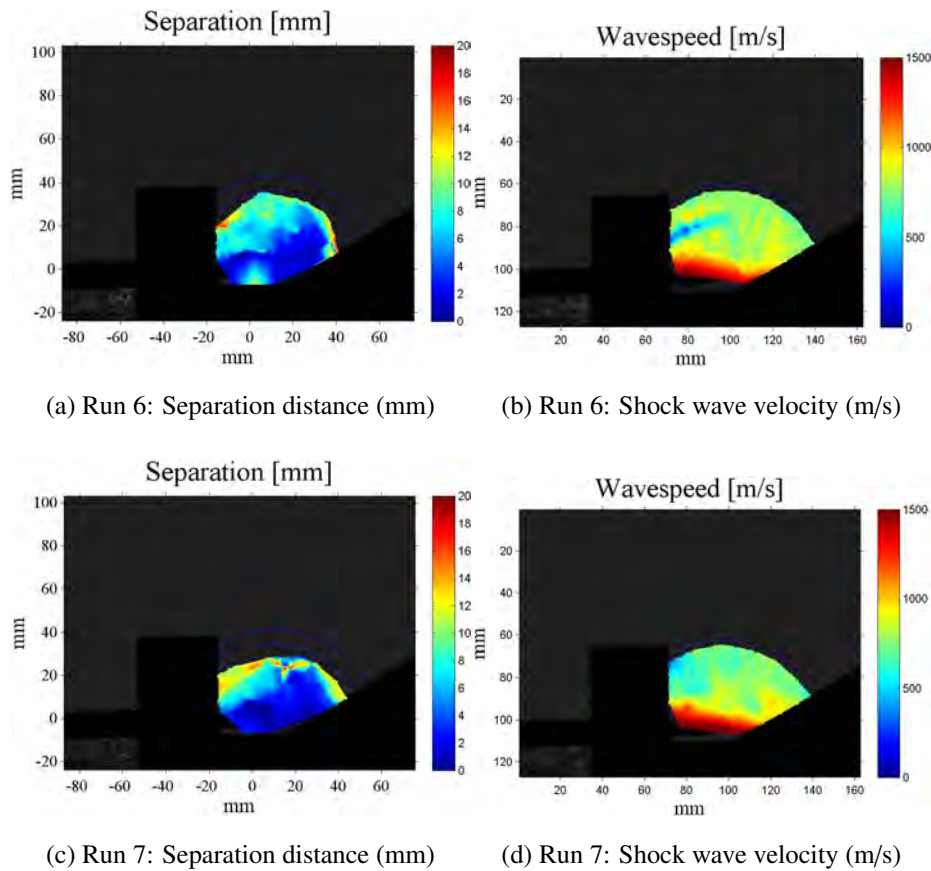e-detonator. When the separation distances are compared to the corresponding velocity plots, the relationship between the exit velocity and the decoupling point can be seen. In Run 5 (Frames (a) and (b) in Fig. 4.23) the velocity profile shows similar velocities to Runs 6 and 7 (Fig. 4.22), but the high velocities are occurring in a circular manner. The velocity profiles for Runs 6 and 7 are flattened and stretching from the pre-detonator exit to the beginning of the wedge. The profile in Run 5 is similar to the exit shape seen during the baseline testing (Fig.: 4.2), for the 22° case. Due to the high velocity in the vertical direction, the flame front decouples before reaching the wedge, and therefore the effects of the wedge are not seen.

Runs 8 and 9 (Fig. 4.23) show the results of not having a high exit velocity. Their velocity profiles (Frames (d) and (f)) show a detonation with velocities of around 1000 m/s (Mach ≈ 2.5); these low velocities cause the wave to decouple. The detonation wave is only coupled for the first 10 mm, and then decouples before reaching the wedge. Due to the low velocities, and their inability to make the transition, it is reasonable to assume that overdriving the wave before exit is critical to achieving a coupled detonation wave in the channel.
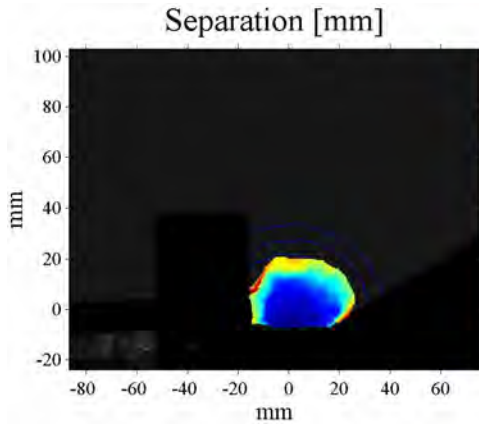
(a) Run 5: Separation distance (mm)
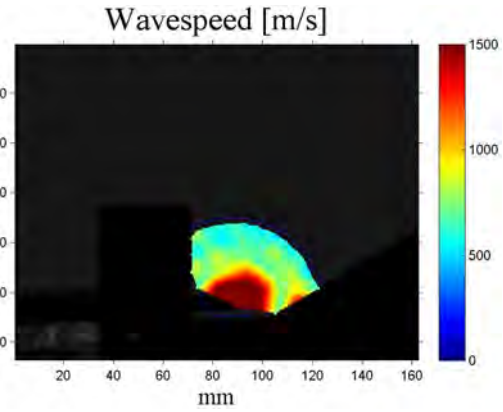
(b) Run 5: Shock wave velocity (m/s)
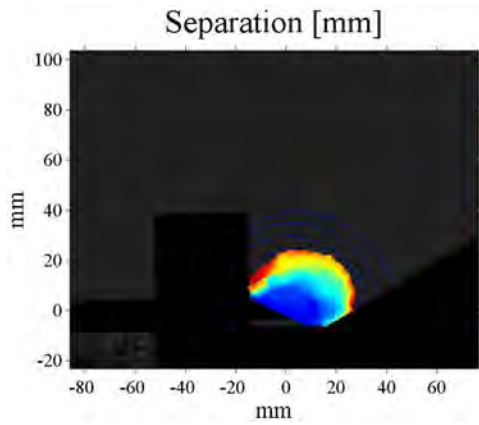
(c) Run 8: Separation distance (mm)

(d) Run 8: Shock wave velocity (m/s)

(e) Run 9: Separation distance (mm)

(f) Run 9: Shock wave velocity (m/s)

Figure 4.23. Separation distance and shock wave velocities for the 30° wedge

4.4.5 45° Wedge

The next wedge tested was 45°. Runs 10-12 (Fig. 4.24) show similar velocity profiles to those seen in Runs 5, 8 and 9 (Fig. 4.23). None of the waves in the 45° runs shown in Fig. 4.24 remain coupled after striking the wedge. During testing, the step change in the pre-detonator had moved slightly with each run to a point where it was no longer effective in overdriving the wave. The step moved to it being secured with only super glue to the inner diamter of the tubing. The tests were re-run as show in Fig. 4.25 after moving the step back to its original location.

(a) Run 10: Separation distance (mm)

(b) Run 10: Shock wave velocity (m/s)

(c) Run 12: Separation distance (mm)

(d) Run 12: Shock wave velocity (m/s)
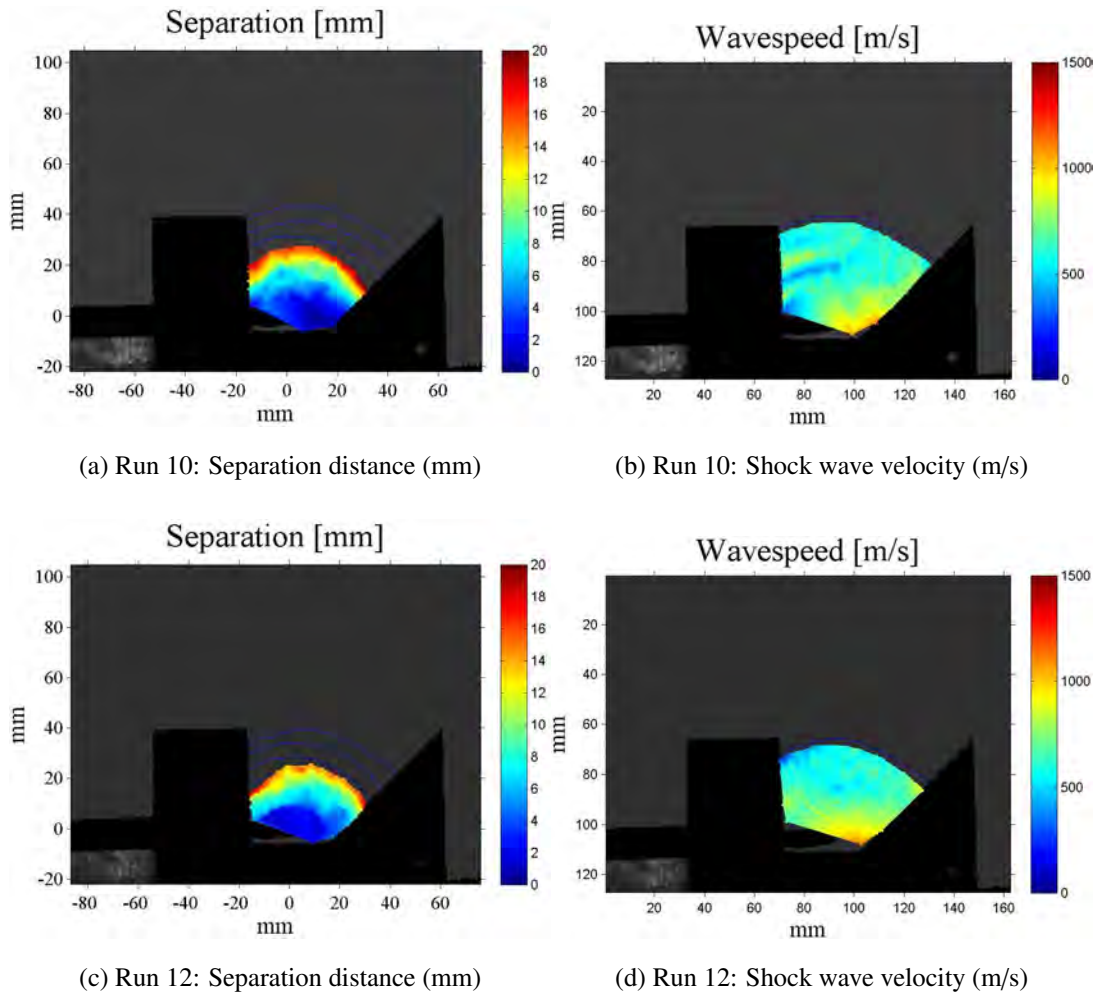
Figure 4.24. Separation distance and shock wave velocities for the 45° wedge

For the remaining tests the fill time for the pre-detonator was increased to 30 ms from 20 ms, for both the hydrogen and oxygen to see if the detonation wave would remain coupled for a longer distance. The increased fill time (Fig. 4.25 and Fig. 4.26) had a favorable effect on the decoupling distance. The setup in Runs 15-17 produced a detonation wave that remained coupled for around 50 mm after exiting the pre-detonator. The increase in the distance traveled is matched with velocity profiles that show a slim, high speed jet exiting the pre-detonator. Once the fill time was increased to 30 ms, the jet was more reliably produced for the remainder of the testing. The increase in fill time most likely led to an increase in oxygen sitting in the pit formed by the wedge in the channel, which would normally decrease the cell size from the hydrogen/air mix in the channel.
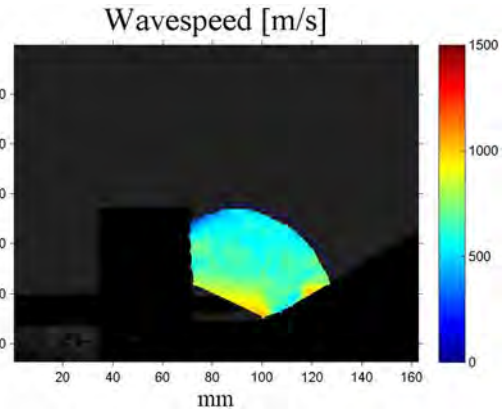

(a) Run 13: Separation distance (mm) (b) Run 13: Shock wave velocity (m/s)

(c) Run 14: Separation distance (mm) (d) Run 14: Shock wave velocity (m/s)
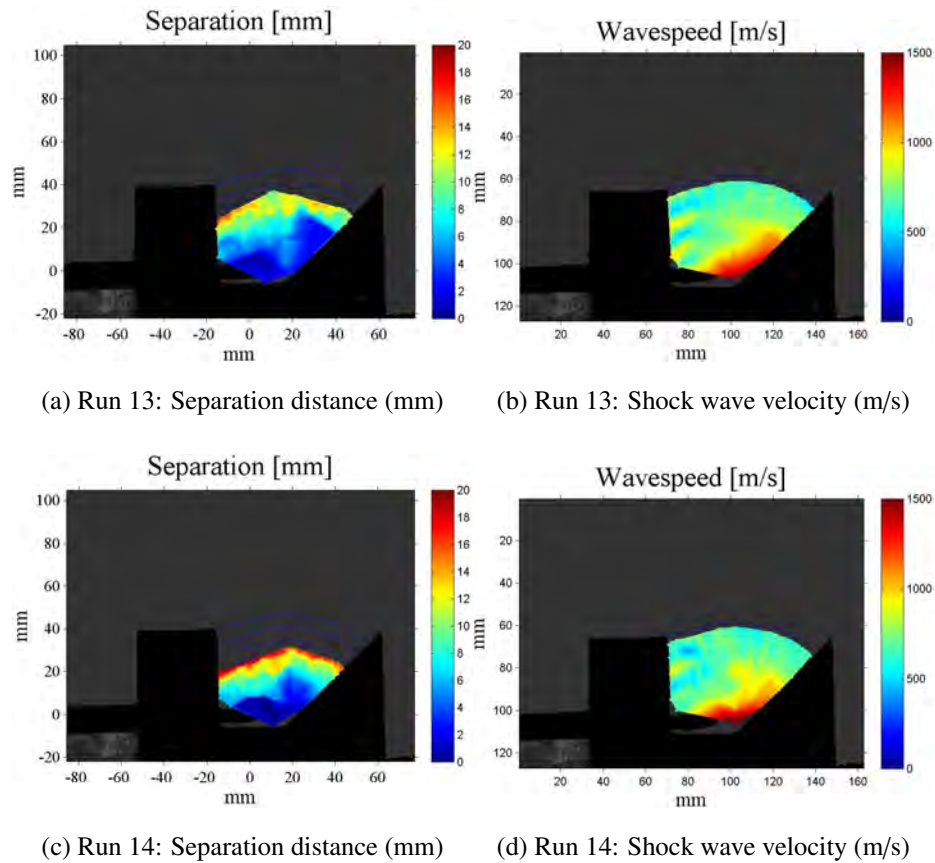
Figure 4.25. Separation distance and shock wave velocities for the 45° wedge
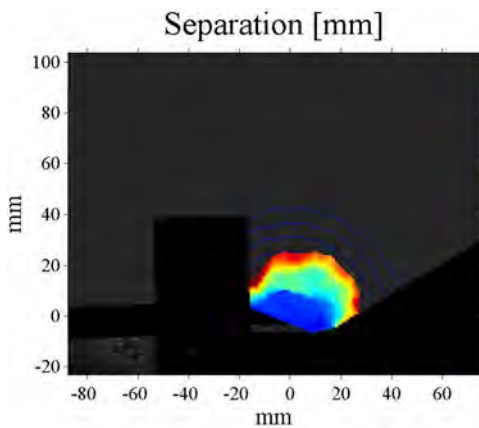
(a) Run 15: Separation distance (mm)

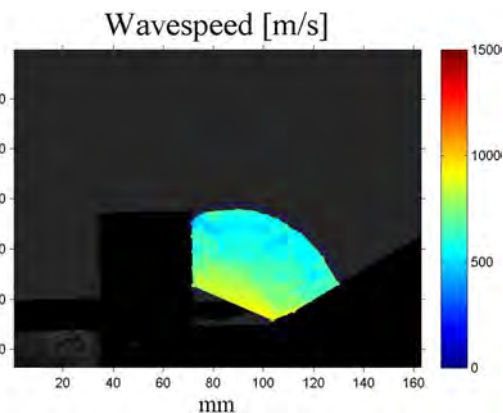(b) Run 15: Shock wave velocity (m/s)

(c) Run 16: Separation distance (mm)

(d) Run 16: Shock wave velocity (m/s)

(e) Run 17: Separation distance (mm)

(f) Run 17: Shock wave velocity (m/s)
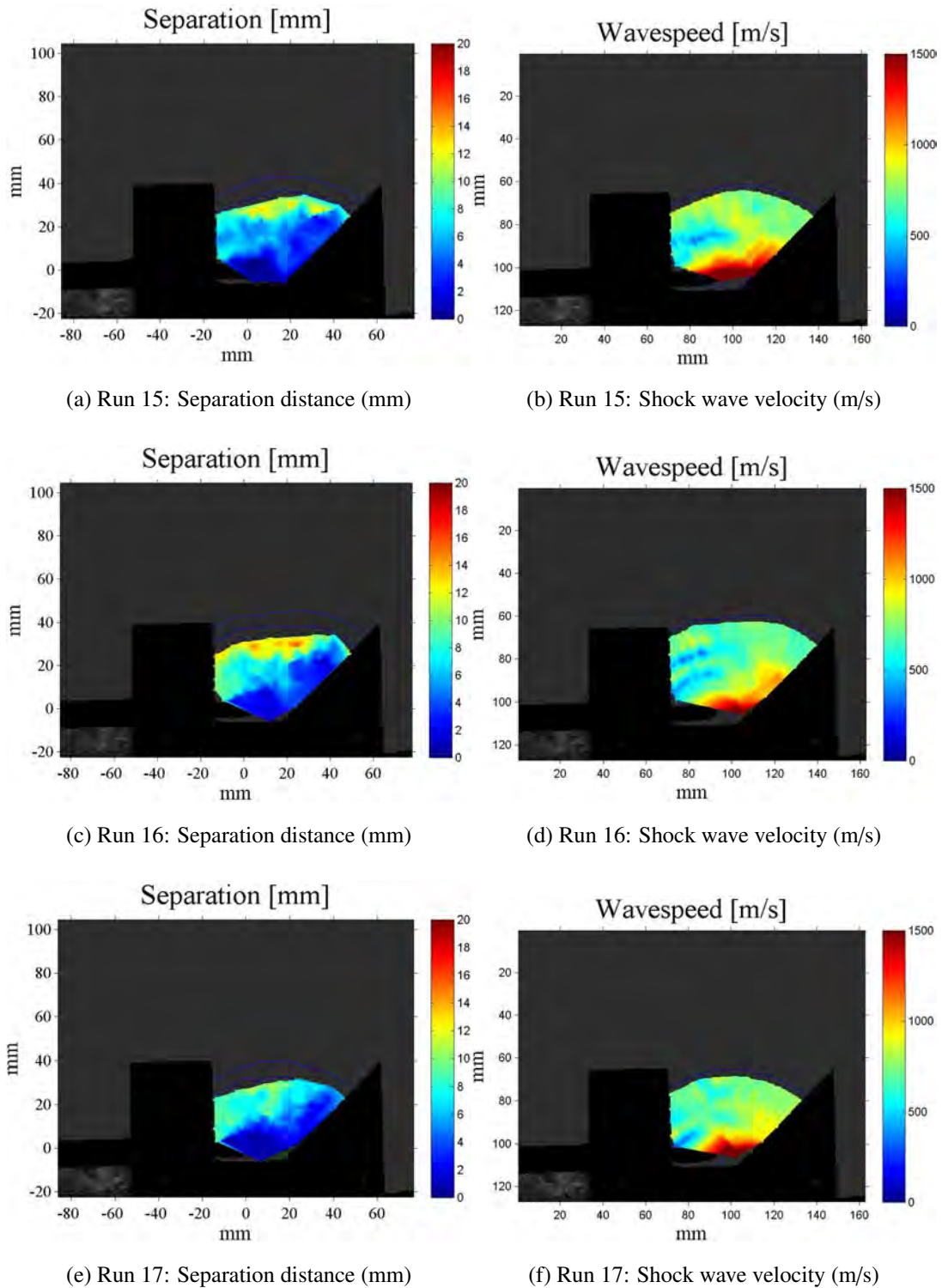
Figure 4.26. Separation distance and shock wave velocities for the 45° wedge

4.4.6   60° Wedge

The final test added a 60° wedge to the channel. The 60° wedge had a beneficial effect in keeping the detonation wave coupled for a longer distance. On average the wave remained coupled for approximately 60 mm from the pre-detonator exit. The wave also re-initiated when turning the corner at the top of the wedge. If the 60° wedge were to be added to the RDE channel, the expansion wave which is created when the detonation turns the corner could help to re-initiate the wave in the correct direction.

(a) Run 18: Separation distance (mm)   (b) Run 18: Shock wave velocity (m/s)

(c) Run 19: Separation distance (mm)   (d) Run 19: Shock wave velocity (m/s)

Figure 4.27. Separation distance and shock wave velocities for the 60° wedge

(a) Run 20: Separation distance (mm)

(b) Run 20: Shock wave velocity (m/s)

(c) Run 21: Separation distance (mm)

(d) Run 21: Shock wave velocity (m/s)

(e) Run 22: Separation distance (mm)
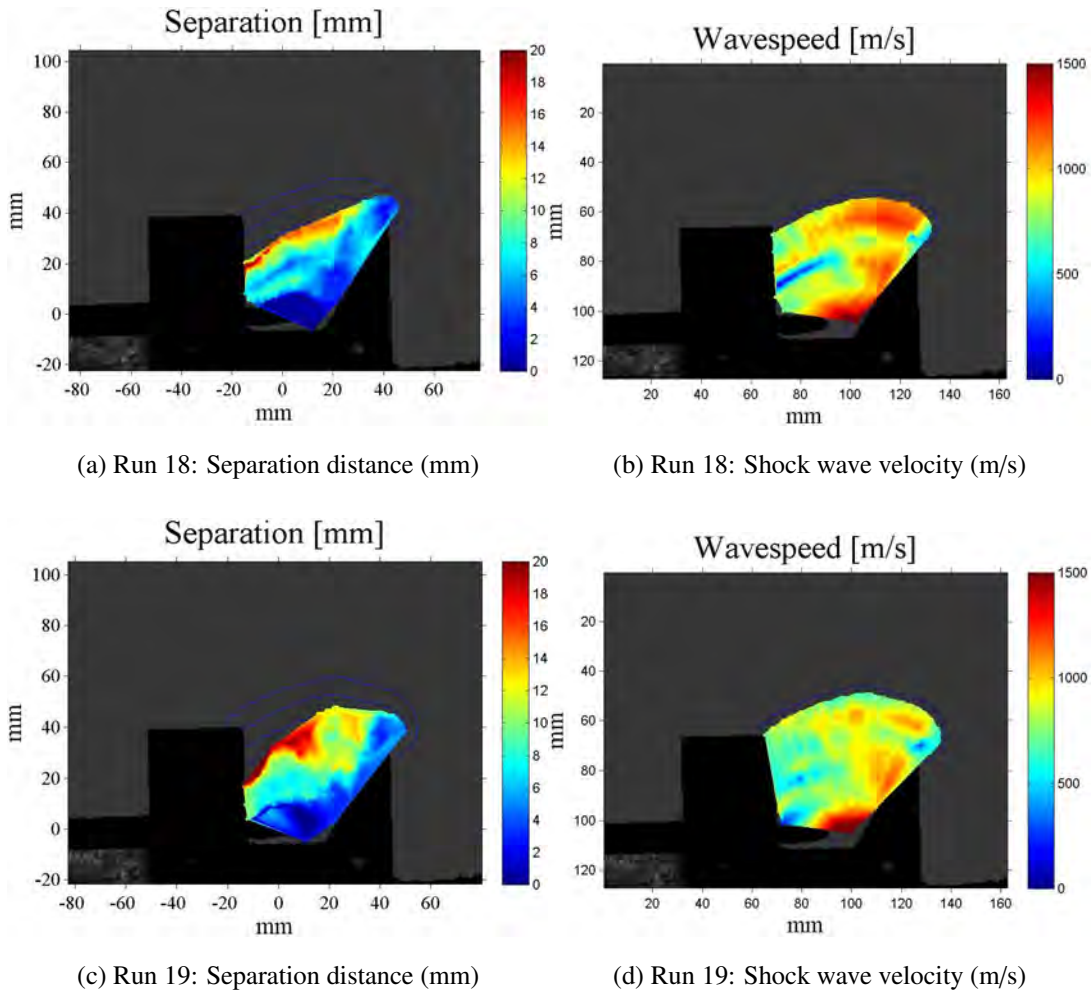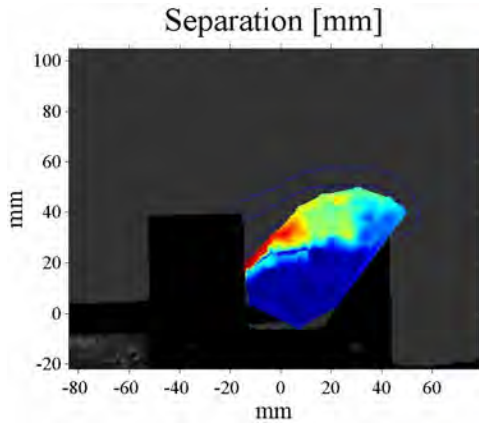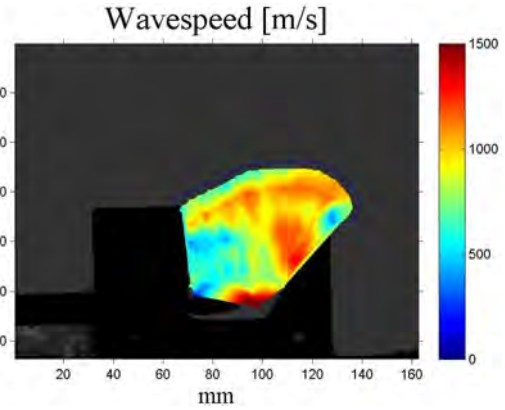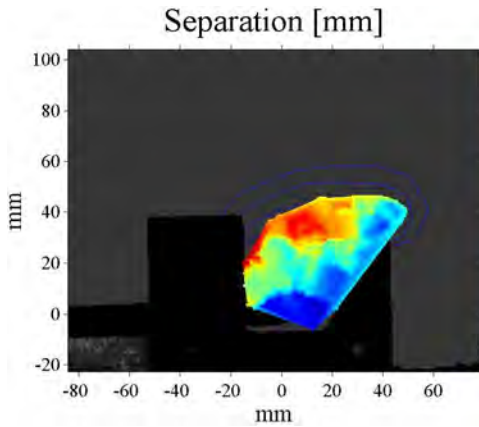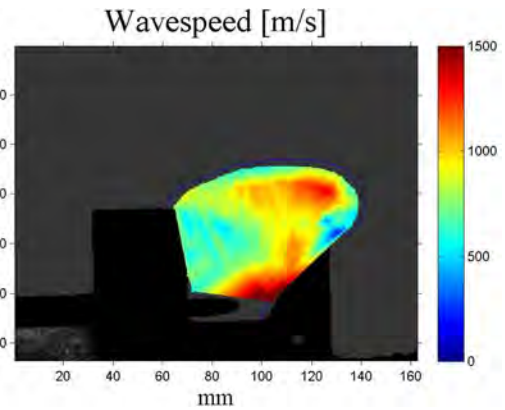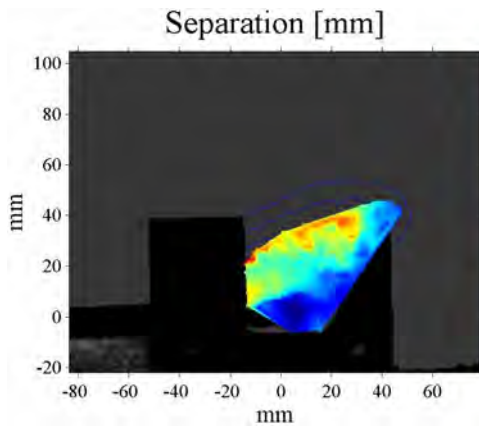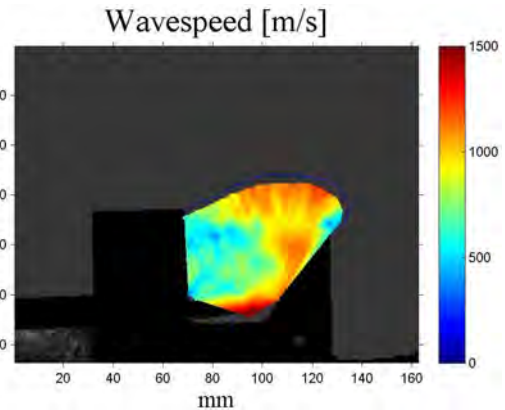
(f) Run 22: Shock wave velocity (m/s)

Figure 4.28. Separation distance and shock wave velocities for the 60° wedge

V. Conclusion

The goal of this research was to develop a means for transitioning a detonation wave from a pre-detonator into an RDE channel. Comparisons were made on decoupling distance and wave velocities for a range of pre-detonator designs, inclination angles, equivalence ratios and geometries placed within the simulated channel. Pre-detonator design research showed that a step change in diameter located 25 mm from the spark plug brought the DDT location from the tube inlet down to under 20 mm from the tests run without the step which had a DDT location between 130 mm and 204 mm. Additionally, a step change insert 25 mm before the exit of the pre-detonator increased exit flow velocities over the regular tubing from approximately 500 m/s to 1000 m/s. Furthermore, because the pre-detonator on the 150 mm RDE is only approximately 63.5 mm in length in its current configuration, the studies would indicate that a detonation wave is not occurring in the pre-detonator. The studies would indicate rather that the pre-detonator is depositing energy into the RDE, which over time builds to a detonation front.

The studies of the simulated RDE channel showed that the detonation wave was decoupling immediately upon exiting the pre-detonator. This research also showed that there is little effect on the decoupling distance by varying the inclination angle of the pre-detonator, as all of the detonation waves decoupled within 25 mm. Adding a step diameter change 25 mm before the exit of the pre-detonator increased the distance the wave remained coupled to 40 mm from the exit into the channel. When the step change was combined with a 60° wedge the wave remained coupled for 60 mm from the pre-detonator exit.

From this research, future RDE designs should implement a step change into the pre-detonator 25 mm from the tube exit. Although the wave decoupled in the simulated channel, if the mass flow and shock wave can be forced in one direction it is hypothesized

that DDT will only occur in one direction, as opposed to both directions. In addition to adding a step, the pre-detonator should be placed immediately above the base plate of the RDE as (Fig. 5.1 (a)). Lowering the pre-detonator would eliminate the shock wave that reflects axially off the base plate. Adding a step change would be a simple addition to the current pre-detonators being used in RDEs.

A more complex solution would be to add the 60° wedge to the base plate where the pre-detonator enters as shown by the red lines in Fig. 5.1 (b). The 60° wedge would provide a stronger directionality to the flow. The 60° wedge also would have the least interaction with the fuel nozzles located on the bottom plate. Further testing under the recommended alterations would help initiate the RDE in a reliable manner.

(a) Simple RDE re-design   (b) Complex RDE re-design
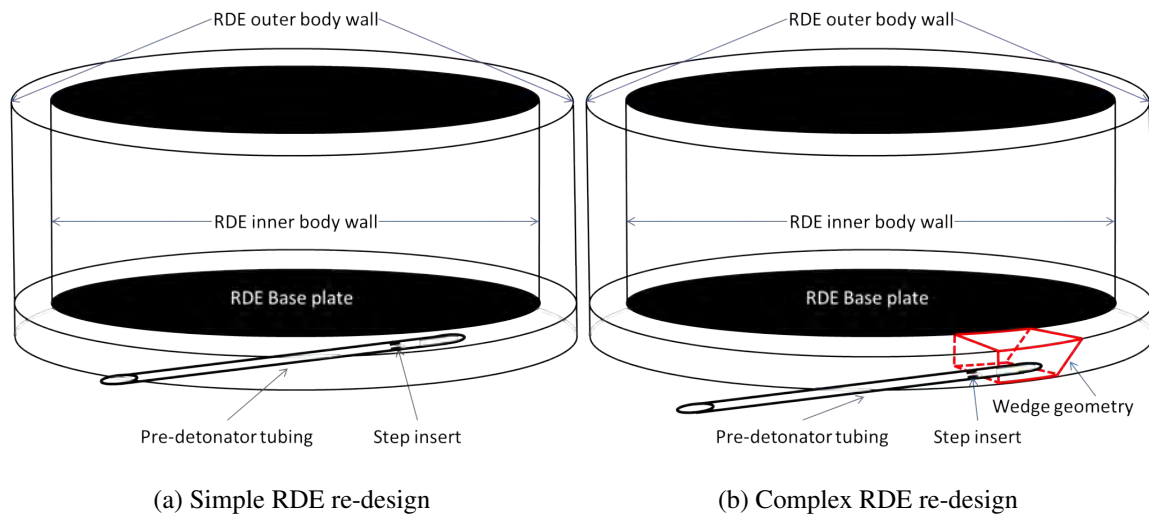
Figure 5.1. Future RDE initiation design

VI. Appendix A - Uncertainty Analysis

Uncertainty analysis was performed for the wave speeds calculated through the use of Schlieren photography. Uncertainty analysis takes into account bias and precision error. The bias uncertainty is made up of the constant error in each measurement system that skews every data point. The precision uncertainty is made up of random error that is introduced at various times throughout the data set. As outlined by Nielsen[28], the bias uncertainty is calculated as the root sum of squares of the estimated error sources as shown in Eqn. 6.1.

$$B = \sqrt{\sum_{k=1}^{k} B_k{}^2} \tag{6.1}$$

The precision uncertainty of each variable is calculated from the standard deviation from a data series as shown in Eqn. 6.2.

$$p = 2\sigma \tag{6.2}$$

The total uncertainty is then found as the root sum of the squares of the bias and precision as shown in Eqn. 6.3.

$$U = \sqrt{B^2 + p^2} \tag{6.3}$$

The uncertainty for the Schlieren videos was primarily a factor of the wave speed at which the velocities were found. Selecting the leading edge of the detonation front added to the bias error. The leading edge of the shock wave was typically 1 pixel wide, while the flame front varied up to 2 pixels. The Phantom v711 camera does not introduce a large amount of error as it has a timing accuracy of up to 20 ns. Equation 6.4 was used to find the bias error.

$$B = \sqrt{\frac{B_{\Delta x}{}^2}{\Delta t} + \frac{\Delta x}{\Delta t^2} B_{\Delta t}{}^2} \tag{6.4}$$

The precision uncertainty develops from the uncertainty in the time between frames and the human error of selecting the correct pixel for the wave front. The human error

83

was estimated to be approximately 0.5 pixels. The error for the camera was found after looking at 20 consecutive frames and finding the average time between frames, the error present was approximately 0.1 μs. Equation 6.5 was used to find the precision error.

$$p = \sqrt{\frac{p_{\Delta x}^2}{\Delta t} + \frac{\Delta x}{\Delta t^2}p_{\Delta t}^2}$$ (6.5)

Table 6.2 is a summary of the errors calculated for the flame front and Tab. 6.1 is a summary of the shock wave error for a range of velocities:

Table 6.1. Error analysis for shock wave

Velocity (m/s)	Bias Error (m/s)	Precision Error (m/s)	Total Error (m/s)
2000	87.4	43.7	97.7
1000	75.7	37.8	84.6
500	72.4	36.2	81.0

Table 6.2. Error analysis for flame front

Velocity (m/s)	Bias Error (m/s)	Precision Error (m/s)	Total Error (m/s)
1200	145.8	38.7	150.9
600	143.5	36.5	148.0
300	142.9	35.8	147.3

As expected the error is higher for the flame front than the shock wave due to its turbulent nature. The error as a percentage increases as the velocity is decreased because the distance moved by the wave over the set 100 μs time frame decreases. Due to the wave moving a smaller number of pixels and the pixel bias error remaining constant, the

error percentage increases. This error was expected and as such the lower velocities should be taken at the readers discretion. More importantly this research focused on separation distance between the shock and flame front. The error present in the distance calculations was dependent on the calibration of the mm/pix. The precision error for the separation distance was approximately 0.05 mm.

VII. Appendix B - Summary of Test Cases

1st Test – 7 Aug 2012 – Simulated RDE Channel

Run	Phi	Inclination	Camera
2	1	45	
3	1	45	
4	1	45	Zoomed
5	.8	45	
6	.8	45	
7	.8	45	
8	.8	45	Zoomed
9	1.2	45	
10	1.2	45	
11	1.2	45	Zoomed
12	1	22	
13	1	22	
14	1	22	Zoomed
15	.8	22	
16	.8	22	
17	.8	22	Zoomed
18	1.2	22	
19	1.2	22	
20	1.2	22	Zoomed
21	1	11	
22	1	11	
23	1	11	Zoomed
24	.8	11	
25	.8	11	
26	.8	11	Zoomed
27	1.2	11	
28	1.2	11	
29	1.2	11	Zoomed

2nd Test – 7 Sep 2012 – 0.25 in Pre-detonator Test

Run	Thread Length (mm)	Step Change?
1	33	Yes
2	33	Yes
3	33	Yes
4	0	No
5	0	No
6	0	No
7	0	No
8	0	No
9	12.7	No
10	12.7	No
11	12.7	No
12	12.7	No
13	25	No
14	25	No
15	25	No

3rd Test – 24 Jan 2013 – 0.5 in Pre-detonator Test

Run	Step at Inlet	Step 25 mm from Exit
1-1	Yes	No
1-2	Yes	No
1-3	Yes	No
1-4	Yes	No
1-5	Yes	No
1-6	Yes	No
1-7	Yes	No
1-8	Yes	No
1-9	Yes	No
2-1	Yes	Yes
2-2	Yes	Yes
2-3	Yes	Yes
2-4	Yes	Yes
2-5	Yes	Yes
2-6	Yes	Yes
2-7	Yes	Yes
2-8	Yes	Yes
2-9	Yes	Yes

4th Test – 6 Feb 2013 – Wedges in Channel Test

Run	Wedge Angle	Fill Time (ms)	Step
1	None	20	Yes
2	None	20	Yes
3	None	20	Yes
4	None	20	Yes
5	30	20	Yes
6	30	20	Yes
7	30	20	Yes
8	30	20	Yes
9	30	20	Yes
10	45	20	Yes
11	45	20	Yes
12	45	20	Yes
13	45	30	Yes
14	45	30	Yes
15	45	30	Yes
16	45	30	Yes
17	45	30	Yes
18	60	30	Yes
19	60	30	Yes
20	60	30	Yes
21	60	30	Yes
22	60	30	Yes

REPORT DOCUMENTATION PAGE

Form Approved
OMB No. 0704–0188

1. REPORT DATE *(DD–MM–YYYY)*	2. REPORT TYPE	3. DATES COVERED *(From — To)*
22–03–2013	Master's Thesis	Oct 2011–Mar 2013

4. TITLE AND SUBTITLE

Design and Testing of an H2/O2 Predetonator for a Simulated Rotating Detonation Engine Channel

5a. CONTRACT NUMBER

5b. GRANT NUMBER

5c. PROGRAM ELEMENT NUMBER

6. AUTHOR(S)

Miller, Stephen J., 2Lt, USAF

5d. PROJECT NUMBER

5e. TASK NUMBER

5f. WORK UNIT NUMBER

7. PERFORMING ORGANIZATION NAME(S) AND ADDRESS(ES)

Air Force Institute of Technology
Graduate School of Engineering and Management (AFIT/EN)
2950 Hobson Way
WPAFB, OH 45433-7765

8. PERFORMING ORGANIZATION REPORT NUMBER

AFIT-ENY-13-M-23

9. SPONSORING / MONITORING AGENCY NAME(S) AND ADDRESS(ES)

Attn: Frederick Schauer
Air Force Research Laboratory
Aerospace Systems Directorate, Turbine Engine Division, Combustion Branch, Advanced Concepts Group
Bldg 71A, D-Bay, 7th St.
Wright Patterson AFB, OH 45433-7251
DSMN 785-6462, frederick.schauer@wpafb.af.mil

10. SPONSOR/MONITOR'S ACRONYM(S)

AFRL/RQTC

11. SPONSOR/MONITOR'S REPORT NUMBER(S)

12. DISTRIBUTION / AVAILABILITY STATEMENT

DISTRIBUTION STATEMENT A:
APPROVED FOR PUBLIC RELEASE; DISTRIBUTION UNLIMITED

13. SUPPLEMENTARY NOTES

This work is declared a work of the U.S. Government and is not subject to copyright protection in the United States.

14. ABSTRACT

A study is presented on the relationship between a pre-detonator and a detonation channel of an RDE. Testing was conducted on a straight narrow channel made of clear polycarbonate windows connected to an H2/O2 pre-detonator to simulate the RDE initiation scheme and allow for flow visualization. A comparison is made on decoupling distance and wave velocities for a range of pre-detonator designs, inclination angles, equivalence ratios and geometries placed within the simulated channel. Regardless of inclination angle or equivalence ratio the detonation wave decoupled within 25 mm from the pre-detonator exit into the channel. A step change in diameter 25 mm from the exit of the pre-detonator increased the coupled distance to approximately 40 mm from the pre-detonator exit. A step diameter change also increased the exit velocity of the wave and directionalized the flow. Wedges of 30°, 45° and 60°, placed in the channel next to the pre-detonator exit, increased the distance the shock and flame remained coupled from the pre-detonator exit to 42 mm, 50 mm and 60 mm, respectively.

15. SUBJECT TERMS

Detonation, Propulsion, Initiation, Rotating

16. SECURITY CLASSIFICATION OF:			17. LIMITATION OF ABSTRACT	18. NUMBER OF PAGES	19a. NAME OF RESPONSIBLE PERSON
a. REPORT	b. ABSTRACT	c. THIS PAGE			Dr. Paul I. King (ENY)
U	U	U	UU	104	19b. TELEPHONE NUMBER *(include area code)* (937)255-6565, ext 4628 (Paul.King@afit.edu)

Standard Form 298 (Rev. 8–98)
Prescribed by ANSI Std. Z39.18